Synthesis, high-field NMR, X-ray structure, and conformational analysis of a 10-membered diamide disulfide ring

Rabindranath B. Maharajh, James P. Snyder, James F. Britten, and Russell A. Bell

Abstract: *N,N'*-[Dimethyl-(2,2'-dithiobisacetyl)]ethylenediamine (**1**) has been synthesized in 30% overall yield from *N,N'*-dimethylethylenediamine and thioacetic acid by an improved procedure involving simultaneous deprotection and oxidative cyclization with iodine. This cyclic diamide disulfide exists in solution as a mixture of two *Z,Z* and one *Z,E* disulfide, and amide ring conformers and has been characterized by nuclear Overhauser effect (NOE), ^1H–^1H, ^1H–^{13}C shift-correlated 2D-NMR and molecular modelling studies. Among the *Z,Z* ring conformers Z,Z_1 and Z,Z_2, the former predominates and interconverts with the latter isomer by rotation about the S—S bond with an activation energy of 14.5 ± 1.3 kcal/mol. Coalescence of N-CH_3 signals occurred at ca. 127°C (500 MHz), which corresponded to an approximate barrier to amide rotation of 19.3 kcal/mol. Aromatic solvent-induced shifts in C_6D_6 corroborated molecular mechanics and NOE predictions of amide stereochemistry. The structure of the *Z,E* stereoisomer of **1** has been determined by single-crystal X-ray diffraction at 296 K. A large geminal N-CH_2 inequivalence (>2 ppm in $CDCl_3$) was observed for the *Z,Z* conformers. Proton chemical shifts have been calculated for the conformers of **1** and related molecular fragments with DFT/GIAO theory. Absolute chemical shifts are modelled within 0.2 ppm of experiment. The unusual nonequivalence of geminal N-CH_2 and S-CH_2 protons can be understood as a combination of shielding mechanisms derived from short N-methyl contacts, amide group orientation, and sulfur lone-pair disposition. An implication of these results is the possibility of using α-C*H* (and eventually α-*C*H) shifts to probe the local conformational space in cyclic peptides and other conformationally constrained rings.

Key words: amide/disulfide rotamers, conformational analysis, density functional theory, DFT/GIAO NMR shift calculations, methylene nonequivalence, molecular modelling.

Résumé : On a synthétisé la *N,N'*-[diméthyl-(2,2'-dithiobisacetyl)]éthylènediamine (**1**), avec un rendement global de 30% à partir de la *N,N'*-diméthyléthylènediamine et de l'acide thioacétique, à l'aide d'une méthode améliorée impliquant une déprotection et une cyclisation oxydante simultanées sous l'influence de l'iode. En solution, ce disulfure diamide cyclique existe sous la forme d'un mélange de deux disulfures *Z,Z* et d'un *Z,E*, en plus des conformères du cycle amide; on l'a caractérisé par effet Overhauser nucléaire (eOn), par des études de RMN 2D avec corrélation de déplacements ^1H–^1H et ^1H–^{13}C et des études de modélisation moléculaire. Parmi les conformères *Z,Z* du cycle, Z,Z_1 et Z,Z_2, le premier est prédominant et les deux subissent une interconversion par le biais d'une rotation autour de la liaison S—S avec une énergie d'activation de 14,5 ± 1,3 kcal/mol. La coalescence des signaux se produit aux environs de 127°C (500 MHz); ceci correspond à une barrière de la rotation de l'amide d'environ 19,3 kcal/mol. Les déplacements induits par un solvant aromatique, C_6D_6, ont permis de confirmer les conclusions de la mécanique moléculaire et les prédictions basées sur l'eOn pour la stéréochimie de l'amide. On a déterminé la structure du stéréoisomère *Z,E* de **1** par diffraction des rayons X par un cristal unique, à 296 K. Avec les conformères *Z,Z*, on a observé une importante inéquivalence géminale pour le N-CH_2 (>2 ppm, dans $CDCl_3$). En se basant sur la théorie de la densité fonctionnelle («DGT/GIAO»), on a calculé les déplacements chimiques des protons des conformères du composé **1** et de fragments moléculaires apparentés. On peut faire la modélisation des déplacements chimiques absolus à 0,2 ppm près des valeurs observées expérimentalement. On peut expliquer la non équivalence exceptionnelle des protons géminés des N-CH_2 et S-CH_2 en se faisant appel à une combinaison de mécanismes de blindage dérivés des contacts à courte distance des N-méthyles, de l'orientation du groupe amide et de l'arrangement de la paire d'électrons non partagée du soufre. Ces résultats impliquent qu'il est possible

Received March 19, 1996.

The authors dedicate this manuscript to the memory of Professor Colin J.L. Lock of McMaster University.

R.B. Maharajh.[1] R&D Laboratory, Nu·Pharm Inc., Richmond Hill, ON L4C 5H2, Canada.
J.P. Snyder. Department of Chemistry, Emory University, Atlanta, GA, 30322, U.S.A.
J.F. Britten and R.A. Bell.[1] Department of Chemistry, McMaster University, Hamilton, ON L8S 4M1, Canada.

[1] Authors to whom correspondence may be addressed. Telephone: R.B.M., (905) 884-0470; R.A.B., (905) 525-9140, ext. 23479. Fax: R.B.M., (905) 884-9876. E-mail: R.B.M., ae149@freenet.hamilton.on.ca

d'utiliser les déplacements des α-C*H* (et éventuellement un α-*C*H) comme sonde pour étudier l'espace conformationnel localisé dans les peptides cycliques ainsi que d'autres cycles conformationnellement restreints.

Mots clés : rotamères amide/disulfure, analyse conformationnelle, théorie de la densité fonctionnelle («DFT/GIAO»), calculs de déplacements chimiques de RMN, non équivalence de méthylènes, modélisation moléculaire.

[Traduit par la rédaction]

Introduction

Structures similar to *N,N'*-ethylenebis(2-thioacetamide) are frequent precursors to complexing reagents for technetium and have been used extensively in Tc-based radioimaging work both at research and clinical levels (1–5). In addition to forming very stable Tc complexes (5), these diamide disulfur (DADS) ligands are highly amendable to modification using standard synthetic techniques and commercial reagents and, as such, represent an attractive ligand system to systematically evaluate structure–activity requirements for the development of tissue-specific technetium chelates. To illustrate, N-C_α carboxylated analogues of DADS ligands are currently being investigated in the targeted delivery of radioactivity in bifunctional chelate strategies (5, 6). However, as examples of ^{99m}Tc radiopharmaceuticals employed for imaging the nonexcretory organs are few, further research in this area is highly desirable. This limited success of existing ^{99m}Tc complexes has been ascribed in part to a lack of sufficient lipid solubility required for adequate membrane transport through capillaries and other lipid barriers (7–9).

In a program to develop cyclic diamide disulfides into lipophilic, bifunctional DADS chelators for ^{99m}Tc radioimaging, we noted the complexity of NMR spectra in a number of nonsymmetric derivatives and the dearth of literature on the conformational properties and a reliable synthetic approach to such compounds. Hence, the preparation of the symmetric diamide disulfide **1** was undertaken as both a conformational and synthetic model and we present herein its synthesis, NMR properties, and solid state and solution state structures. An investigation into the conformational properties of such simple ring systems also allows for a better understanding of peptide conformation and an improved approach towards the rational design of conformationally constrained peptides that possess important biological activities (10).

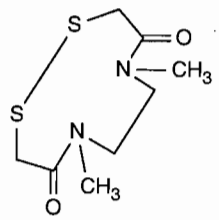

1

Results and discussion

Synthesis

The 10-membered heterocycle **1** was synthesized from 2-mercaptoacetic acid and *N,N'*-dimethylethylenediamine in four steps in 30% overall yield as shown in Scheme 1. Tritylation of thioacetic acid under Lewis acid catalysis readily afforded the *S*-protected acid **2**, which was subsequently reacted with 1,3-dicyclohexylcarbodiimide (DCC) and *N*-hydroxysuccinimide (NHS) to give the activated ester **3**. Treatment of two equivalents of **3** with *N,N'*-dimethylethylenediamine in dry dimethoxyethane allowed for the acylation of both nitrogens and the formation of the diamide **4** in 76% yield. Deprotection of **4** was effected with 1.1 equivalents of iodine in ethanol–acetonitrile and, by maintaining high dilution conditions to preclude intermolecular disulfide formation, in situ intramolecular oxidative cyclization readily generated the monomeric disulfide **1** in 66% yield.

The choice of the *S*-protecting group for thioacetic acid and the method for its cleavage were crucial for the efficiency of the synthesis. The S atom in these compounds is normally protected as aryl thioethers, hemithioacetals, or thioesters (11); however, deprotection frequently requires harsh conditions that can lead to decomposition when sensitive functional groups are present. Moreover, the sulfur products of these acidic or basic deprotection schemes can also engage in side reactions, including acid-catalyzed *N*- to *S*-acyl transfer initiated by SH attack to neighbouring amide groups[2] and disulfide polymerization via thiolate coupling (14, 15). The instability of unprotected sulfur atoms compounded with harsh deprotection methods makes this synthetic strategy less desirable for the development of radioimaging precursors.

For the development of chemically sensitive radiopharmaceuticals incorporating the DADS ligand, an exceedingly mild *S*-deprotection method was required. Iodine has been used in the removal of trityl groups from sulfur with facile, in situ oxidation to acyclic disulfides (16). Moreover, disulfides are stable, readily prepared, and easy to cleave with mild reductants (for example, $SnCl_2$) and as such represent attractive precursors to Tc chelants, particularly in the clinical setting. The synthesis was therefore undertaken with trityl as the sulfur protecting agent and iodine as the deprotectant.

Conformational analysis

(a) ^{1}H and ^{13}C NMR data

The product (**1**) ran as one spot when examined by thin-layer chromatography and melted over a 1.0°C range, indicating good sample homogeneity. Infrared, Raman, and mass spectra of the product were consistent with its proposed monomeric structure (see Experimental methods). The ^{1}H and ^{13}C NMR

[2] Decomposition of C_{11} substituted DADS fatty acid amide conjugates has been noted in our lab during *S*-detritylation using the CF_3COOH–Et_3SiH method (12). This is suspected to proceed via nucleophilic attack of the unmasked SH group to the C=O function at the C_{11} amide, resulting in a six-membered thiolactone and the corresponding 11-amino fatty acid. This mechanism is based on analogy to ref. 13.

Scheme 1.

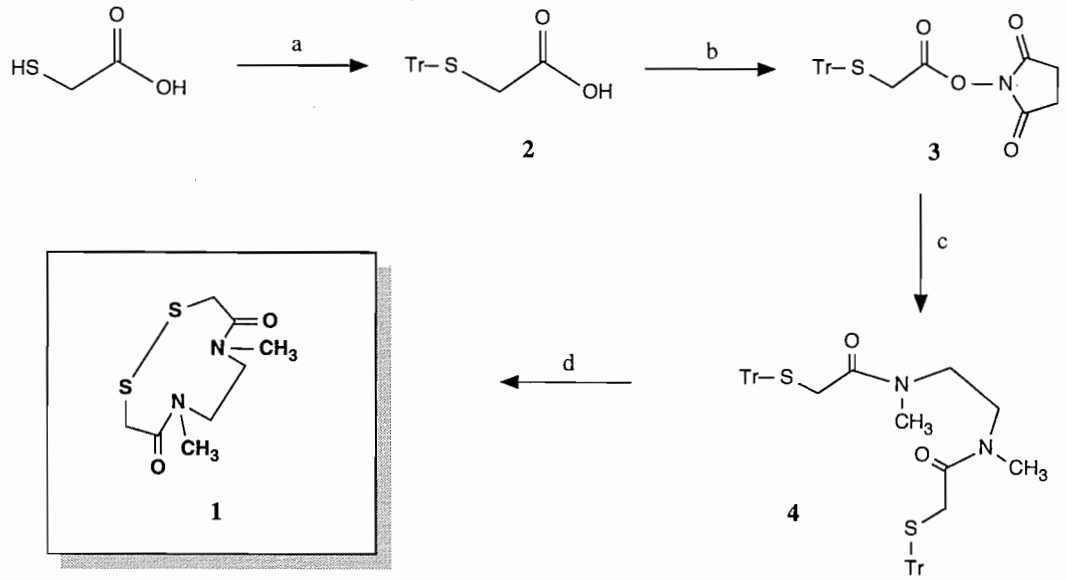

(a) Ph_3C-OH, BF_3·etherate, AcOH, 70°C; (b) NHS, DCC, dry DME, 0–5°C; (c) 0.5 equiv. $CH_3NHCH_2CH_2NHCH_3$, NEt_3, AN; (d) I_2, AN/EtOH, [**4**] = 5mM. NHS = *N*-hydroxysuccinimide; DCC = *N,N'*-dicyclohexylcarbodiimide; DME = dimethoxyethane; AN = acetonitrile.

analyses (Fig. 1 and Tables 1 and 2), however, showed dramatically complex signal profiles despite the established chemical purity of the sample and its symmetry-related, isolated sets of ^1H and ^{13}C nuclei. That this multiplicity of lines arose from the presence of different ring conformers was suggested from the ^{13}C spectrum, which showed 12 lines (Table 2) in the aliphatic region (δ 30–50) rather than the anticipated three.[3] This increased number of lines was rationalized by noting that each amide group can exist in either *Z* or *E* stereochemistry because of restricted amide rotation: this enables the cyclic disulfide to adopt, in principle, three conformations with the amide groups *Z,Z*, *Z,E*, and *E,E*.

(b) ^1H dynamic NMR studies

Variable-temperature ^1H NMR was employed to determine the presence of conformational isomers. Spectra recorded in the temperature range −61.5 to 30.0°C in $CDCl_3$ indicated that the proposed conformers were in slow exchange at room temperature and below. At higher temperatures in DMSO-d_6, interconversion rates increased, as evidenced from the gradual coalescence of all resonances (Fig. 2). However, it was not possible to observe the three signals expected in the regime of fast exchange at 500 MHz, as this would require heating the sample to an impractically high level.

To further confirm the exchange process as restricted amide rotation, the free energy of activation, $\Delta G^{\ddagger}$, was estimated using a modified form of the Eyring formulation (17):

$$[1] \quad \Delta G^{\ddagger} = RT_c[22.96 + \ln(T_c/\Delta\nu)]$$

The coalescence temperature T_c was estimated from Fig. 2 to be about 127°C at 500 MHz, based on the coalescence of the singlets at 2.42 and 2.71 ppm.[4] This afforded $\Delta G^{\ddagger}_{127} \approx 19.3$ kcal/mol. The measured barrier is consistent with those typically reported for substituted *N,N'*-dimethylamides (e.g., dimethylacetamide, $\Delta G^{\ddagger}_{25.2} = 17.4$ kcal/mol; dimethylpropanamide, $\Delta G^{\ddagger}_{25.2} = 16.7$ kcal/mol) (18). Restricted rotation associated with the S—S linkage (19, 20)[5] and ring inversion presumably contributes to this composite $\Delta G^{\ddagger}$, thus magnifying it in relation to typical acyclic amide rotational barriers.

A heteronuclear ^1H–^{13}C 2D NMR shift-correlated experiment at room temperature identified the geminal pairs of diastereotopic protons for *three* geometric isomers and, with the aid of standard chemical shifts, permitted the location of their NCH_2CH_2N groupings (Fig. 3). Two of these appeared as sets of A_2B_2 (or AA'BB') spin systems in the F_1 (^1H) domain, consistent with two symmetrical isomers, and the third as a more complex ABCD spin system for an unsymmetrical isomer. The experiment also enabled the assignment of carbon signals associated with the three isomers. The ^1H–^1H connectivity patterns in each isomer were confirmed through a homonuclear 2D COSY-45 NMR experiment (data not shown).

The data from the 2D and dynamic NMR (DNMR) experiments, as well as patterns in signal multiplicity, were fully consistent with the presence of three, interconvertible, conformational isomers of **1** at room temperature. The amide configurations of these ring conformers have been assigned as Z,Z_1, *Z,E*, and Z,Z_2. The designation Z,Z_1 refers to the major *Z,Z* ring conformer while Z,Z_2 indicates the minor one. These proposed

[3] Signal averaging for lengthy periods revealed the presence of additional signals, which presumably arises from trace amounts of other ring conformers.

[4] Later ascribed to the N-CH_3 resonances of the unsymmetrical *Z,E* ring isomer.

[5] The barrier to S—S rotation in the ring conformers Z,Z_1 and Z,Z_2 is addressed later on.

Fig. 1. The 500 MHz ^{1}H NMR spectrum of **1** in $CDCl_3$ at 303 K between 2.5 and 5.0 ppm.

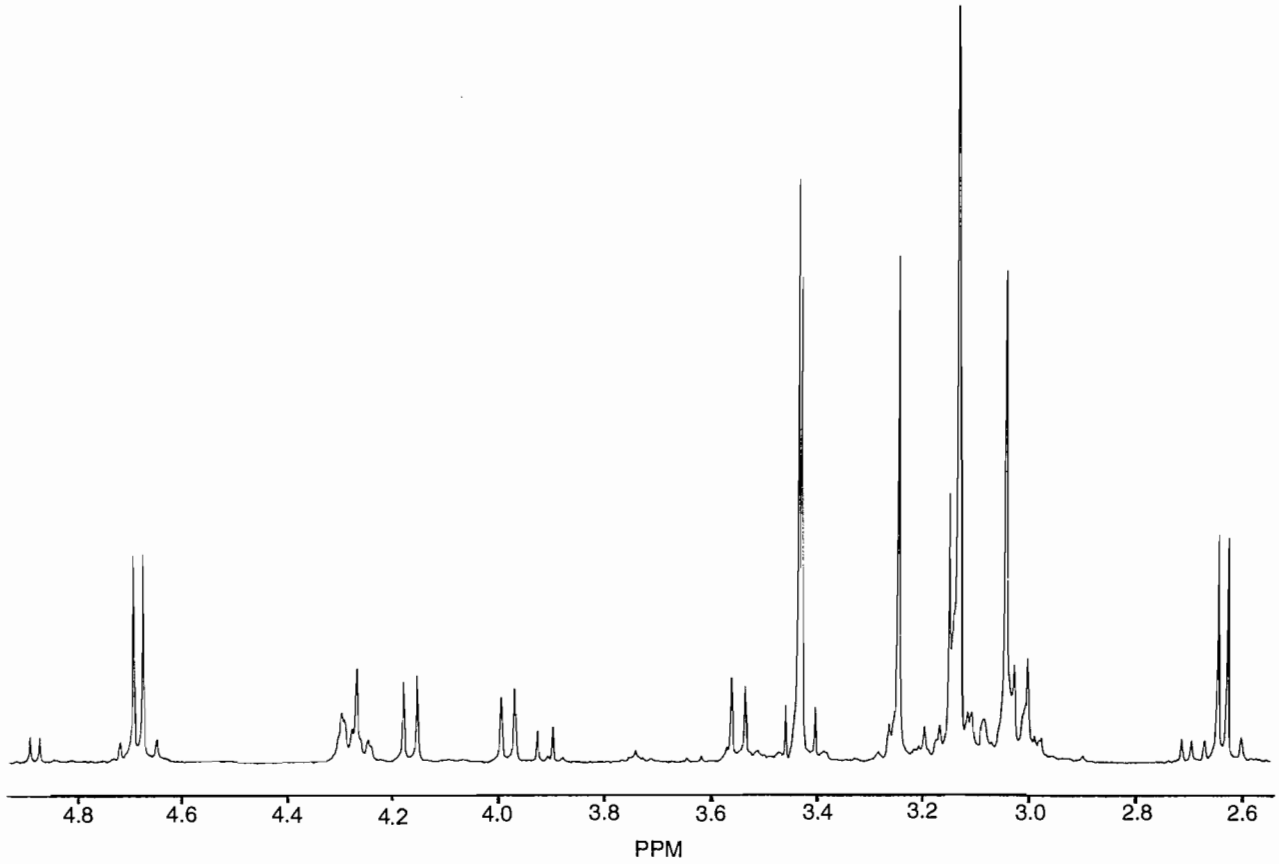

geometries have been shown to be consistent with the results of other experiments, including benzene dilution ^{1}H NMR shifts, nuclear Overhauser effect (NOE) experiments, single-crystal X-ray diffraction studies, molecular modelling, and proton shielding calculations (vide infra).

Proton integrals and ^{13}C resonance intensities (Tables 1 and 2) suggested the following stability trend among the conformers: $Z,Z_1 > Z,E > Z,Z_2$. This finding can be rationalized from an analysis of the sterically driven, conformational preferences governing *N,N'*-dialkylamides: for large-membered lactams, the *Z* stereochemistry is energetically favored over *E* (21). Therefore, the *Z* configuration in **1** can be expected to be the predominant amide stereochemistry in solution. Based on the ratio of intensities of the N-CH_3 ^{13}C signals (Table 2) and, assuming a Boltzmann population distribution at 303 K, the Z,Z_1 ring conformer was favored over the *Z,E* by 0.61 kcal/mol and *Z,E* over the Z,Z_2 by 0.87 kcal/mol. Table 3 presents the corresponding percentage compositions in $CDCl_3$, as well as in DMSO-d_6 and C_6D_6 solvents. The results suggest that the isomeric composition of **1** appeared to be relatively independent of solvent.

The most noteworthy feature in the NMR spectrum of **1** is the large geminal shift differences ($\Delta\delta_{OBS}$) between the N-CH_2 protons of the *Z,Z* and, to a lesser extent, *Z,E* conformers. In $CDCl_3$, the largest $\Delta\delta_{OBS}$ was measured at 2.17 ppm for the minor Z,Z_2 isomer, while the Z,Z_1 and *Z,E* configurations recorded 2.04, 1.18, and 1.26 ppm, respectively (Table 1). The chemical shift differences were invariant with the concentration of **1** in $CDCl_3$, precluding any effects due to intermolecular association. These results suggested that the N-CH_2 (and S-CH_2) groups in the symmetrical *Z,Z* isomers are pairwise

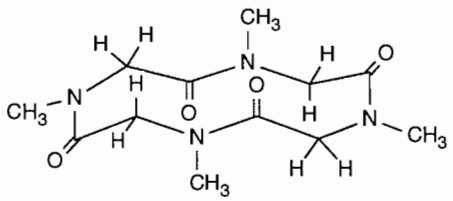

5

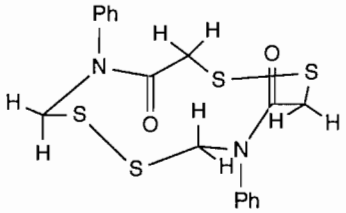

6

Table 1. 500 MHz ^{1}H NMR assignments (ppm (multiplicity, integral,[a] amide stereochemistry[b])) for **1** in $CDCl_3$ at 303 K.

	Conformer		
Signal	Z,Z_1	Z,E	Z,Z_2
N-CH_3	3.13(s,~6H)	3.04(s,~3H,*E*) 3.24(s,~3H,*Z*)	3.15(s,~6H)
N-$(CH_2)_2$	2.64(dd,2H)[c] 4.68(dd,2H)[c] ^2J = −13.7 Hz[e] $^3J_{ax\text{-}ax}$ = 11.2 Hz[f] $^3J_{ax\text{-}eq}$ = 4.8 Hz $^3J_{eq\text{-}eq}$ = 1.4 Hz	3.01(m,~1H,*Z*)[c] 4.27(obs[d] m,~1H,*Z*)[c] ^2J = −14.41 Hz 3.09(obs m,~1H,*E*)[c] 4.27(obs m,~1H,*E*)[c] $^3J_{ax\text{-}ax}$ = 11.6 Hz $^3J_{eq\text{-}ax}$ = 3.6, 3.9 Hz $^3J_{eq\text{-}eq}$ = 2.4 Hz	2.71(dd,2H)[c] 4.88(dd,2H)[c] ^2J = −13.5 Hz $^3J_{ax\text{-}ax}$ = 11.1 Hz $^3J_{ax\text{-}eq}$ = 5.1 Hz $^3J_{eq\text{-}eq}$ = 1.3 Hz
S-CH_2	3.42(AB d,2H)[c] 3.45(AB d,2H)[c] ^2J = −12.7 Hz	3.55(AB d,1H,*E*)[c] 3.99(AB d,1H,*E*)[c] ^2J = −13.2 Hz 3.03(obs AB d,~1H,*Z*)[c] 4.16(AB d,1H,*Z*)[c] ^2J = −12.8 Hz	3.19(obs AB d,~2H)[c] 3.91(AB d,2H)[c] ^2J = −14.7 Hz

[a]Integrals are relative within a conformer series.
[b]Assignments of amide stereochemistry was based on NOE, MM2, and X-ray crystallographic data.
[c]Geminally coupled (determined from ^{1}H–^{13}C chemical shift correlated experiment).
[d]Obscured.
[e]All ^2J couplings were assumed to be negative.
[f]All ^3J couplings were measured from MMX-calculated structures.

Table 2. 126 MHz *J*-modulated ^{13}C NMR assignments (ppm (relative intensity, amide stereochemistry[a])) for **1** in $CDCl_3$ at 303 K.

	Conformer		
Signal	Z,Z_1	Z,E	Z,Z_2
N-CH_3	36.58(–98)	33.59(–17,*E*) 41.17(–18,*Z*)	37.10
S-CH_2	36.98(144)	37.49(31,*Z*) 42.17(20,*E*)	40.69(18)
N-$(CH_2)_2$	44.23(127)	48.20(26) 48.99(22)	46.17(16)
CO-NH	166.55(14)	168.84(6) 169.46(5)	—

[a]Stereochemical assignments are based on the analysis of NOE and ^{1}H–^{13}C shift correlated data.

equivalent or enantiotopic and that the N-CH_2 protons have markedly different magnetic environments. Large geminal proton chemical shift differences have been observed in a few semi-rigid, polyamide systems (22–24). In cyclotetrasarcosyl, **5**, the isochronous pairs of the *N*-methylene protons are separated by about 2 ppm (in $CDCl_3$) (23), while one set of those for the tetrathiacyclododecane **6** have a chemical shift difference of 1.78 ppm (in $CDBr_3$) (24).

Invariably, such large (i.e., >1.5 ppm) N-carbinyl splittings appear to be associated with the sterically favored *Z* amide stereochemistry, which places these protons in or close to the respective amide planes pointing toward the C=O groups

Fig. 2. 500 MHz ^{1}H NMR variable temperature spectra of **1** in DMSO-d_6.

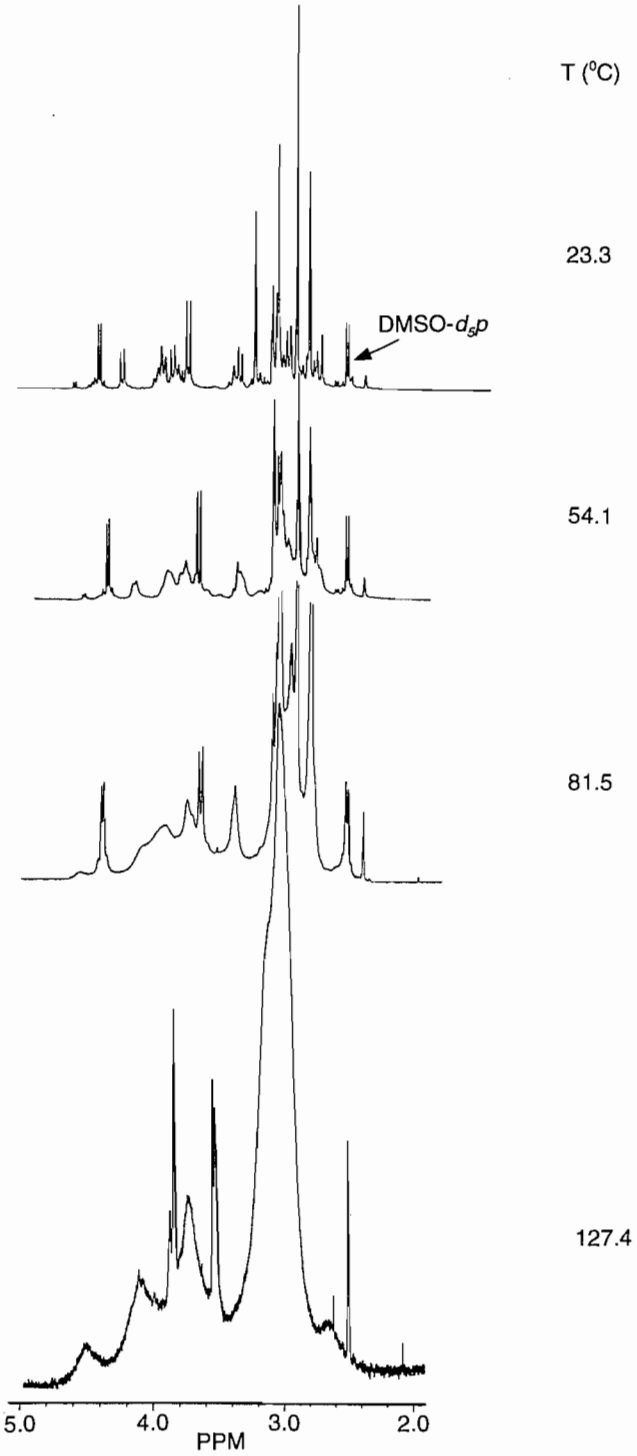

(25).

(c) NOE data

To further define the solution state conformations of **1**, NOE experiments were carried out in $CDCl_3$ at 303 K on signals of the two major isomers. Representive difference NOE spectra for these isomers are shown in Figs. 4 and 5. The inserts illustrate NOE interactions for a given geometric isomer, together with their interatomic distances as determined from MM2-calculated structures.

Fig. 3. ^{1}H-^{13}C chemical shift correlated spectra of **1** in DMSO-d_6 at 303 K. The diastereotopic N-CH_2 protons of the *Z,Z* isomers are circled.

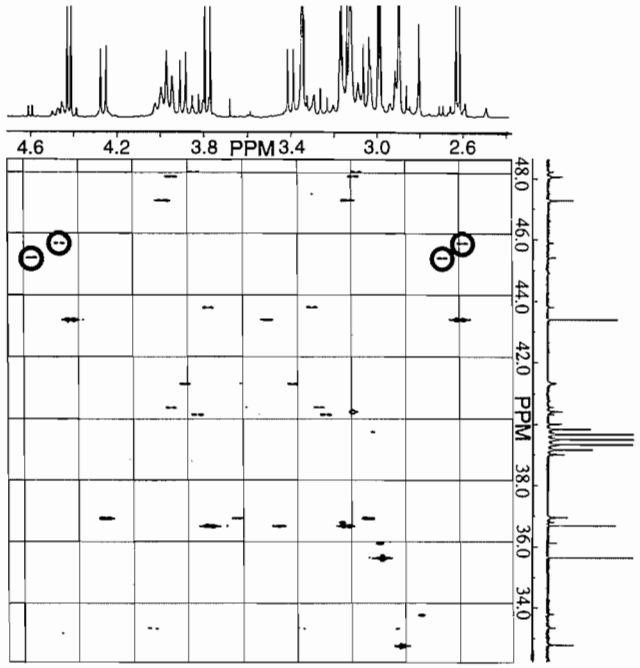

In the major isomer, irradiation of the AB S-CH_2 quartet at 3.43 ppm resulted in a large NOE of the *N*-methyl protons at 3.13 ppm (Fig. 4(*a*)), indicative of a pseudoaxial S-C*H* and N-CH_3 proximity about a *Z* amide configuration. This enhancement was not expected for an *E* stereochemistry, as a larger distance would separate the appropriate protons. The observation of a NOE between the shielded N-CH_2 (2.64 ppm) and N-CH_3 protons (Fig. 4(*b*)) was consistent with a *Z* geometry, where the former protons occupy a pseudoequatorial position *syn* to the adjacent CH_3 group. Irradiation of the N-CH_3 resonance caused NOEs at not only the expected positions of the shielded N-CH_2 and S-CH_2 protons, but also at the deshielded N-C*H* at 4.68 ppm (Fig. 4(*c*)). The weaker enhancement of the deshielded N-C*H* (relative to the shielded protons) suggested a transannular proximity with its *opposite* N-CH_3 group — an interaction made possible through pseudoaxial configurations[6] for both groups. Thus, a C_2 symmetric *Z,Z* conformation best matched the NOE observations noted for the major solution conformation of **1** (see **1a**, Fig. 8).

In the nonsymmetric isomer, irradiation of the S-C*H* signal at 3.55 ppm induced a strong enhancement of its geminal partner at 3.99 ppm as well as a weaker enhancement of the N-CH_2 protons at 4.27 ppm (Fig. 5(*a*)). According to molecular models, the latter NOE was only possible between the pseudoaxial S-C*H* (H(3b)) and the pro-*R* N-C*H* (H(6b))

[6] N-CH_2 protons that occupy either pseudoaxial or pseudoequatorial positions in the symmetrical *Z,Z* isomers are denoted as H_{ax} or H_{eq}, respectively.

Table 3. Calculated and observed population distributions for conformers Z,Z_1, Z,E, and Z,Z_2 at 303 K.

Conformer	Calcd. E_{Steric} (kcal/mol)	Calcd. population distribution (%)[a]	Observed population distributions[a,b] (%)		
			$CDCl_3$	DMSO-d_6[c]	C_6D_6
Z,Z_1 (**1a**)	0	82	53	54	54
Z,E (**1c**)	2.03	3	39	29	38
Z,Z_2 (**1b**)	1.15	15	8	6	8

[a]According to the Boltzmann relationship: $n_2/n_1 = \exp(-\Delta G/RT)$, T = 303 K.
[b]Based on ^{1}H NMR integrals.
[c]Small amounts (<12%) of additional conformers were detected and measured using ^{13}C NMR intensities.

Fig. 4. 500 MHz NOE difference spectra (*a*)–(*c*) of the Z,Z_1 stereoisomer of **1** in $CDCl_3$ at 303 K. The irradiated peak is indicated at the arrowed frequency.

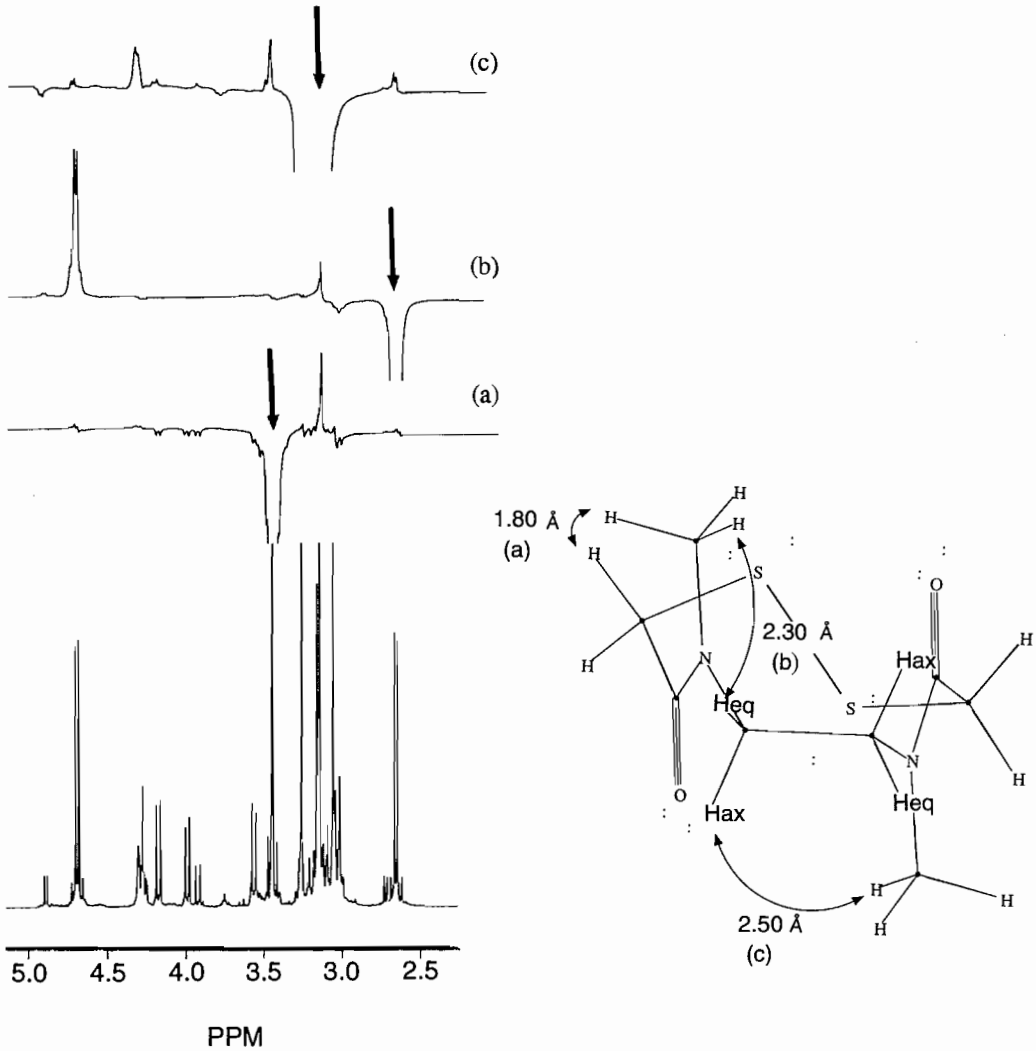

about the *E* amide group. The X-ray structure and molecular mechanics calculations (Figs. 6 and 8, **1c**) supported this result: with an interatomic separation of 1.97 Å, the electron clouds of these protons were overlapping by about 0.4 Å. The positive N-CH_3 enhancement at 3.24 ppm was most likely a result of saturation transfer (26) to S-C*H* (H(10a)) at 4.16 ppm by which it is strongly relaxed (Fig. 5(*c*)). Barring geminal enhancements, NOEs were not observed for the second *E* S-C*H* (H(3a)) signal at 3.99 ppm: this was consistent with a pseudoequatorial position (Fig. 5(*b*)).

Fig. 5. 500 MHz NOE difference spectra (*a*)–(*d*) of the *Z,E* stereoisomer of **1** in $CDCl_3$ at 303 K. The irradiated peak is indicated at the arrowed frequency.

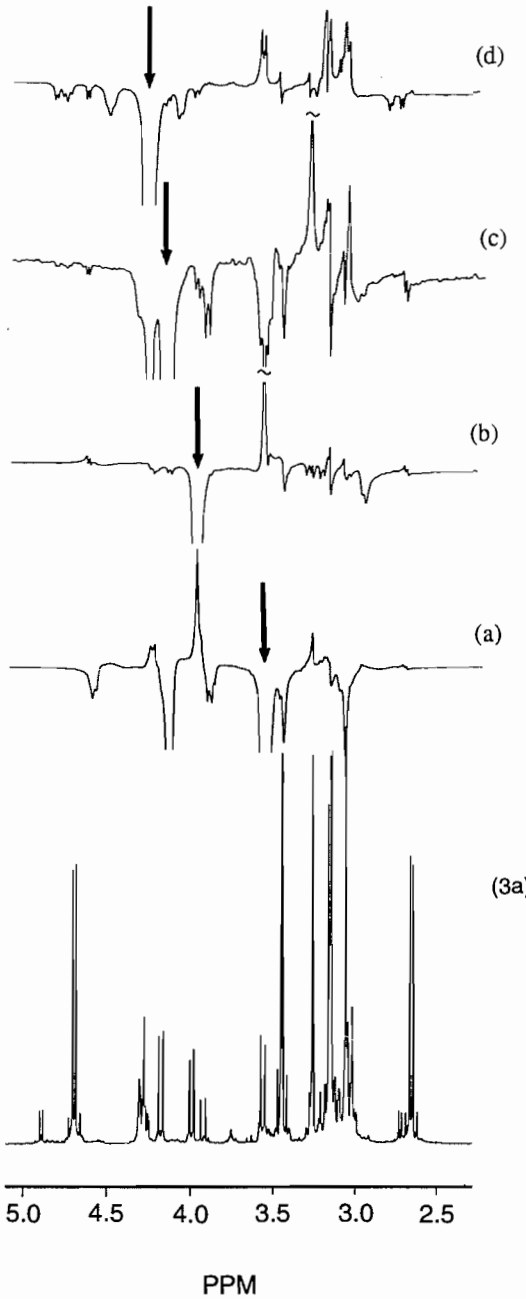

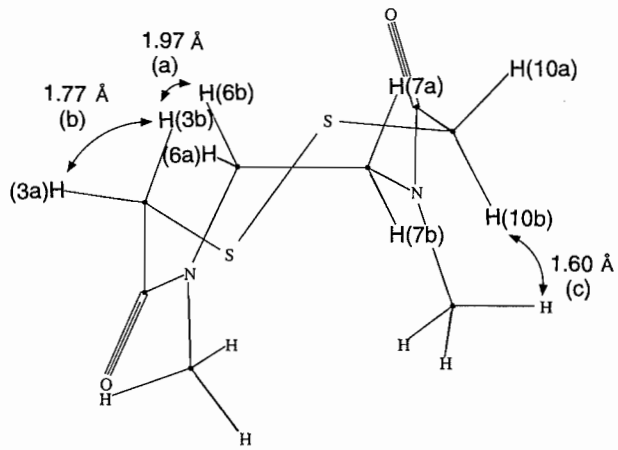

Irradiation of the S-C*H* (H(10a)) resonance at 4.16 ppm (Fig. 5(*c*)) induced strong enhancement of the downfield N-CH_3 protons at 3.24 ppm, which was indicative of a di-pseudoaxial disposition of protons about a *Z* amide bridge. Examination of the *Z,E* molecular model revealed that the point of closest approach of these protons was ca. 1.6 Å. The NOE was therefore consistent with a *Z* amide stereochemistry and supported the prediction (27) that the *downfield* N-CH_3 (and N-CH_3 by ^1H–^{13}C shift correlation, Fig. 3) belonged to the *Z* amide group in the *Z,E* conformer.

Irradiating the co-resonating, downfield N-CH_2 protons (H(6b) and H(7a)) at 4.27 ppm created moderate NOEs at 3.55, 3.10, and 3.01 ppm (Fig. 5(*d*)). The 3.55 ppm enhancement arises from interaction of H(6b) with H(3b) (as in Fig. 5(*a*)). The latter two enhancements most likely arose from geminal interactions with the shielded *Z* and *E* N-CH_2 protons (H(7b) and H(6a), respectively) and was further evidence that the nonsymmetric component of **1** (see **1c**, Fig. 8) possessed a *Z,E* geometry.

Unfortunately, it was not possible to obtain definitive NOE data for the Z,Z_2 isomer, largely because of its low abundance and intensity complications arising from saturation transfer from more abundant isomers. Although saturation transfer effects were also observed for the *Z,E* and, to a lesser extent,

Fig. 6. The crystal structure of the *Z,E* isomer of **1**. 30% probability thermal ellipsoids are shown for non-hydrogen atoms.

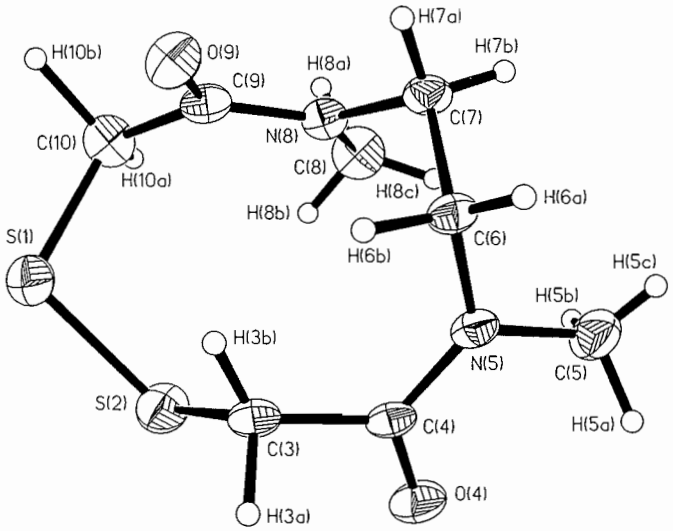

the Z,Z_1 conformers, their relatively intense signals allowed for the extraction of useful conformational information from their NOE spectra.

(d) Aromatic solvent-induced shift (ASIS) studies

The lack of NOE data for the Z,Z_2 stereoisomer prompted an ASIS investigation to determine its solution state geometry. Studies on a variety of amides (28–31) have consistently showed that aromatic solvents shift the signals of the N-C_α protons *trans* to the carbonyl group *upfield* to a greater extent than those at the *cis* position. By comparison of their relative proton shifts in aromatic and nonaromatic solvents, these resonances can be assigned to a particular amide stereochemistry.

The ^{1}H NMR spectrum of **1** in benzene-d_6 revealed that the N-CH_3 (and N-CH_2) resonances of both major (Z,Z_1) and minor (Z,Z_2) isomers exhibited very similar upfield aromatic solvent-induced shifts (0.56 and 0.61 ppm relative to the $CDCl_3$ shifts, data not shown). Since the NOE experiments confirmed the major isomer to have the *Z,Z* geometry, the benzene dilution experiments suggested that the minor isomer also possesses the *Z,Z* configuration. The relatively large ASIS values were also consistent with a *Z* geometry (32). An *E,E* stereochemistry in the minor isomer would have resulted in a smaller ASIS value and an increased separation between the N-CH_3 resonances of the major and minor isomers upon benzene-d_6 dilution. It is worth noting that in benzene-d_6, the N-CH_2 splittings for the Z,Z_1 and Z,Z_2 ring conformers increased to 2.58 and 2.69 ppm, respectively.

(e) Solid state structure analysis

An X-ray diffraction study of **1** was undertaken to establish unambiguously the geometry that could give rise to the enormous NMR shift differences observed for the geminal methylene protons.

The geometry and numbering of the X-ray structure of **1** is shown in Fig. 6; atomic coordinates, bond length, and bond angles are listed in Tables 4–8. As the structure analysis revealed, **1** crystallized with the *Z,E* geometry. This was a surprising result since NMR data had shown the Z,Z_1 isomer to be the dominant geometry in solution (Table 3). A survey of the bond angles and bond lengths of **1** indicated no unusual deviations from normal values. The disulfide and amide torsional angles (Table 7) are very close to ground state values (i.e., 90° and planarity, respectively) indicating low torsional strain in the *Z,E* ring.

Table 4. Atomic coordinates ($\times 10^4$) and equivalent isotropic displacement coefficients ($Å^2 \times 10^3$).

Atom	*x*	*y*	*z*	U_{eq}[a]
S(1)	2354(2)	581(2)	1211(1)	57(1)
S(2)	1815(2)	2637(2)	2470(1)	56(1)
C(3)	2612(7)	4613(7)	1793(5)	40(2)
C(4)	3905(7)	6481(7)	2911(4)	37(2)
O(4)	3040(6)	6847(6)	3814(3)	55(2)
N(5)	5926(6)	7663(5)	2905(4)	38(2)
C(5)	7114(9)	9380(8)	4057(5)	60(3)
C(6)	7089(7)	7342(7)	1883(4)	37(2)
C(7)	8656(7)	6622(7)	2219(5)	39(2)
N(8)	7584(6)	4821(5)	2511(3)	35(2)
C(8)	7751(9)	4980(8)	3888(5)	55(3)
C(9)	6531(7)	3148(7)	1506(5)	39(2)
O(9)	6581(6)	3115(5)	382(3)	50(2)
C(10)	51177(9)	1295(8)	1766(5)	49(3)

[a]Equivalent isotropic *U* defined as one third of the trace of the orthogonalized U_{ij} tensor.

Table 5. Bond lengths (Å) with estimated standard deviations in parentheses.

Bond	Length	Bond	Length
S(1)—S(2)	2.035(2)	S(1)—C(10)	1.835(6)
S(2)—C(3)	1.836(6)	C(3)—C(4)	1.517(6)
C(4)—O(4)	1.229(7)	C(4)—N(5)	1.342(6)
N(5)—C(5)	1.468(6)	N(5)—C(6)	1.461(7)
C(6)—C(7)	1.520(9)	C(7)—N(8)	1.466(7)
N(8)—C(8)	1.479(7)	N(8)—C(9)	1.353(5)
C(9)—O(9)	1.234(7)	C(9)—C(10)	1.515(8)

The unit cell contains two *Z,E* molecules of **1**, which are related by a center of inversion. Molecules stack in columns with a high degree of packing efficiency given the unsymmetrical nature of the *Z,E* isomer. The most significant intermolecular contact is O(4)···C(8), which is 3.23 Å. Intramolecular nonbonding contacts were observed between O(9) and H(7a), and between H(3b) and H(6b). These nuclei, separated by 2.35 Å and 2.01 Å, respectively, are within the sum of the accepted van der Waals radii for oxygen and hydrogen (1.4–1.6 and 1.2 Å, respectively) (33, 34). These contacts may contribute to the rather large NMR shift differences observed for geminal hydrogen nuclei of the *Z,E* conformation (vide infra).

The excellent agreement between the crystal structure of the *Z,E* isomer and the NOE-derived conformational model established a link to proton shift assignments. The direction and magnitude of proton shifts may be qualitatively explained by the positions of the geminal protons relative to

Table 6. Bond angles (deg) with estimated standard deviations in parentheses.

Bond	Angle	Bond	Angle
S(2)-S(1)-C(10)	104.0(2)	S(1)-S(2)-C(3)	104.4(2)
S(2)-C(3)-C(4)	106.6(4)	C(3)-C(4)-O(4)	117.6(4)
C(3)-C(4)-N(5)	120.5(4)	O(4)-C(4)-N(5)	122.0(4)
C(4)-N(5)-C(5)	117.2(4)	C(4)-N(5)-C(6)	125.8(3)
C(5)-N(5)-C(6)	116.9(4)	N(5)-C(6)-C(7)	112.9(4)
C(6)-C(7)-N(8)	111.4(4)	C(7)-N(8)-C(8)	117.1(3)
C(7)-N(8)-C(9)	117.7(4)	C(8)-N(8)-C(9)	125.1(5)
N(8)-C(9)-O(9)	121.3(5)	N(8)-C(9)-C(10)	119.2(5)
O(9)-C(9)-C(10)	119.4(4)	S(1)-C(10)-C(9)	108.8(5)

Table 7. Torsional angles (deg) with estimated error in parentheses.

Bond	Angle	Bond	Angle
C(10)-S(1)-S(2)-C(3)	85.9(0.3)	S(2)-S(1)-C(10)-C(9)	−69.2(0.4)
S(2)-S(1)-C(10)-H(10A)	61.7(0.4)	S(2)-S(1)-C(10)-H(10B)	−170.5(0.3)
S(1)-S(2)-C(3)-C(4)	−135.8(0.3)	S(1)-S(2)-C(3)-H(3A)	115.4(0.3)
S(1)-S(2)-C(3)-H(3B)	−5.9(0.3)	C(8)-N(8)-C(9)-O(9)	−175.1(0.6)
C(8)-N(8)-C(8)-H(8B)	−43.3(0.9)	C(7)-N(8)-C(9)-O(9)	4.5(0.8)
C(7)-N(8)-C(9)-C(10)	−172.4(0.5)	C(9)-N(8)-C(8)-H(8B)	−43.2(0.9)
C(9)-N(8)-C(8)-H(8C)	−162.3(0.5)	C(9)-N(8)-C(8)-H(8A)	59.1(0.6)
C(7)-N(8)-C(8)-H(8B)	137.2(0.6)	C(7)-N(8)-C(8)-H(8C)	18.1(0.8)
C(7)-N(8)-C(8)-H(8A)	−120.5(0.5)	C(9)-N(8)-C(7)-C(6)	79.8(0.6)
C(9)-N(8)-C(7)-H(7A)	−32.4(0.7)	C(9)-N(8)-C(7)-H(7B)	−154.5(0.5)
C(8)-N(8)-C(7)-C(6)	−100.5(0.5)	C(8)-N(8)-C(7)-H(7A)	147.2(0.5)
C(8)-N(8)-C(7)-H(7B)	25.1(0.7)	C(4)-N(5)-C(6)-C(7)	−102.5(0.6)
C(4)-N(5)-C(6)-H(6A)	131.9(0.6)	C(4)-N(5)-C(6)-H(6B)	20.4(0.8)
C(5)-N(5)-C(6)-C(7)	74.1(0.6)	C(5)-N(5)-C(6)-H(6A)	−51.5(0.7)
C(5)-N(5)-C(6)-H(6B)	−163.0(0.5)	C(6)-N(5)-C(4)-O(4)	179.5(0.6)
C(6)-N(5)-C(4)-C(3)	0.3(0.9)	C(5)-N(5)-C(4)-O(4)	2.9(0.9)
C(5)-N(5)-C(4)-C(3)	−176.3(0.6)	C(6)-N(5)-C(5)-H(5A)	143.4(0.6)
C(6)-N(5)-C(5)-H(5B)	−111.0(0.6)	C(6)-N(5)-C(5)-H(5C)	11.4(1.1)
C(4)-N(5)-C(5)-H(5A)	−39.7(0.9)	C(4)-N(5)-C(5)-H(5B)	65.9(0.7)
C(4)-N(5)-C(5)-H(5C)	−171.8(0.8)	N(5)-C(6)-C(7)-N(8)	57.5(0.4)
N(5)-C(6)-C(7)-H(7A)	174.3(0.3)	N(5)-C(6)-C(7)-H(7B)	−67.1(0.5)
H(6A)-C(6)-C(7)-N(8)	−176.0(0.4)	H(6A)-C(6)-C(7)-H(7A)	−59.2(0.5)
H(6A)-C(6)-C(7)-H(7B)	59.4(0.6)	H(6B)-C(6)-C(7)-N(8)	−66.0(0.5)
H(6B)-C(6)-C(7)-H(7A)	50.8(0.5)	H(6B)-C(6)-C(7)-H(7B)	169.4(0.4)
N(8)-C(9)-C(10)-S(1)	109.0(0.5)	N(8)-C(9)-C(10)-H(10A)	−12.6(1.0)
N(8)-C(9)-C(10)-H(10B)	−144.2(0.5)	O(9)-C(9)-C(10)-S(1)	−68.1(0.7)
O(9)-C(9)-C(10)-H(10A)	170.4(0.6)	O(9)-C(9)-C(10)-H(10B)	38.8(0.7)
O(4)-C(4)-C(3)-S(2)	−58.2(0.7)	O(4)-C(4)-C(3)-H(3A)	59.5(0.7)
O(4)-C(4)-C(3)-H(3B)	−174.1(0.6)	N(5)-C(4)-C(3)-S(2)	121.0(0.5)
N(5)-C(4)-C(3)-H(3A)	−121.3(0.6)	N(5)-C(4)-C(3)-H(3B)	5.2(1.0)

their adjacent carbonyl group: in general, a proton will be increasingly deshielding as it approaches the plane and (or) midpoint of a carbonyl group (25). In the *Z* amide system, H(7a) and H(7b) (see Fig. 6) are 10.4° and 13.9° out of the amide plane defined by atoms O(9)-C(9)-N(8) and are located 2.36 and 3.36 Å, respectively, from the midpoint of the C═O bond. Thus, H(7a) should resonate *downfield* (4.27 ppm) from H(7b) (3.01 ppm). Similarily, H(6b) and H(6a) of the *E* amide are 170.6° and 151.6° removed from the O(4)-C(4)-N(5) plane and are situated at distances of 3.27 and 3.65 Å, respectively, from the midpoint of the carbonyl bond. Since H(6b) is "closer" to its adjacent amide group, it should appear downfield (4.27 ppm) of its geminal partner (3.09 ppm). It is interesting to note that the very similar deshielding influences on H(7a) and H(6b) appear to result from two different orientations of the protons, namely, H(7a) is close to the O atom of one C═O group, while H(6b) is near the C atom of the other. The ab initio shift calculations (see Table 12) provided addi-

Fig. 7. The 25 MHz CP-MAS ^{13}C spectrum of **1** at 303 K.

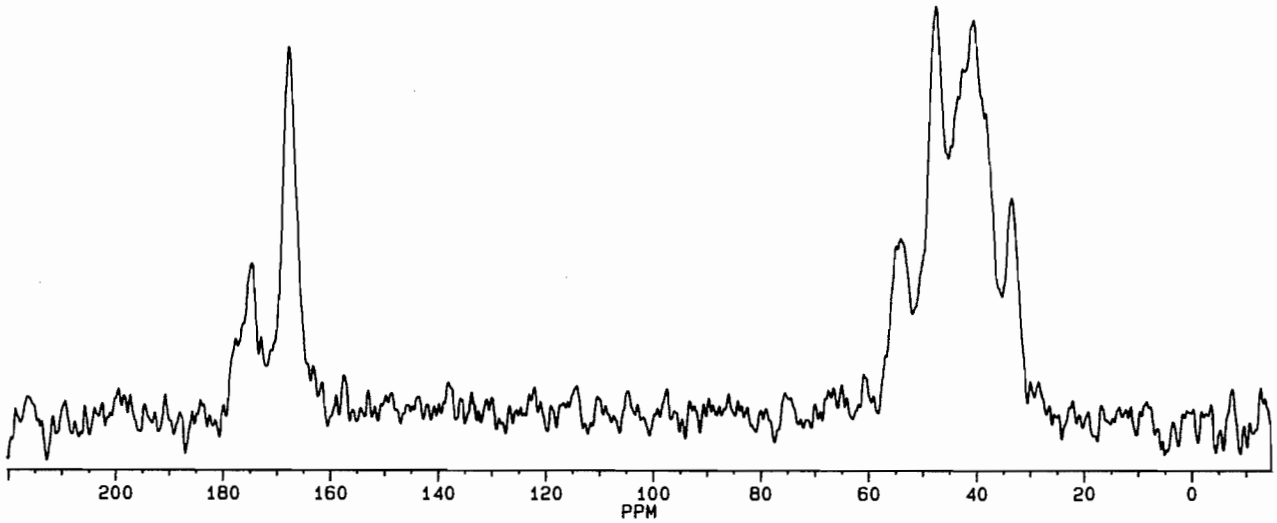

Table 8. Hydrogen atom coordinates ($\times 10^4$) and equivalent isotropic displacement coefficients ($Å^2 \times 10^3$).

Atom	*x*	*y*	*z*	*U*
H(3A)	1310	4855	1499	80
H(3B)	3234	4124	1042	80
H(5A)	6271	10070	4465	80
H(5B)	7334	8860	4893	80
H(5C)	8323	10241	4063	80
H(6A)	7774	8433	1645	80
H(6B)	5952	6293	960	80
H(7A)	9204	6338	1359	80
H(7B)	9867	7622	2946	80
H(8A)	8451	4127	3840	80
H(8B)	6348	4137	3992	80
H(8C)	8162	6271	4375	80
H(10A)	5285	1229	2691	80
H(10B)	5578	231	904	80

tional confirmation of the above qualitative assessment of proton assignments.

To further assess the relationship between the solution and solid state geometries of **1**, the cross-polarization, magic angle spinning (CP-MAS) ^{13}C NMR spectrum of a larger sample of crystalline **1** (0.10 g) was determined in the solid state at 25.2 MHz (Fig. 7). Unfortunately, excessive broadening of the ^{13}C resonances caused by dipolar coupling to ^{14}N nuclei, as well as signal overlap and sensitivity complications, prevented an unequivocal correlation of characteristic shifts between the solid state and solution state spectra in the 30–50 ppm range. Spectra recorded at a higher field and (or) higher sample concentration would probably resolve this inadequacy.

An interesting outcome of the solid state experiment, however, was noted in the carbonyl region: two broad signals of unequal intensity (167.30 and 174.39 ppm) suggested the presence of at least two conformers in the sample. If the recrystallized sample of **1** consisted *only* of the *Z,E* geometric isomer, then only two, *equally intense* resonances should be observed for the carbonyls. Based on chemical shift and intensity comparisons with the solution state ^{13}C data (Table 2), the more intense signal at 167.30 ppm was ascribed to the Z,Z_1 structure, while the unresolved resonance at 174.39 ppm was assigned to the *Z,E* conformer. The observation of two species in the solid state NMR could be rationalized by the presence of both *Z,Z* and *Z,E* crystals in the sample. The rather high barriers to amide isomerization could promote the crystallization of the *Z,Z* and *Z,E* amide ring conformers into *separate* lattice structures. Examples of acyclic monoamides have been reported to crystallize in either the *Z* or *E* geometry, with only one geometric rotamer in each unit cell (35).

Computational analysis

While the X-ray structure provided a link between the ^1H NMR chemical shift and geometry for the *Z,E* isomer, no such benefits were available for the *Z,Z* isomers. Consequently, a number of computational methods were investigated to aid in chemical shift assignment and to provide insight into the origins of the unusually large N-CH_2 anisochronism and its apparent absence for the S-CH_2 protons.

(a) MMX calculations

Molecular mechanics calculations were performed using PCMODEL (version 4.0) to evaluate the conformational geometries and energies of the Z,Z_1 and Z,Z_2 structures. From over 90 unique starting geometries, five conformers were found for **1** within 5 kcal/mol of the global minimum structure (Table 9, Fig. 8). Conformers **1a** (*Z,Z*), **1b** (*Z,Z*), and **1c** (*Z,E*) agreed well with the structural models inferred from NOE, thermodynamic, X-ray, and NMR symmetry data. Based on this correlation, the observed conformers in the NMR spectra of **1** — Z,Z_1, Z,Z_2, and *Z,E* — were proposed to have similar structures as **1a**, **1b**, and **1c**, respectively.

The *Z,E* isomer (Fig. 6) was taken as the source of the unsymmetrical set of NMR resonances and, among the set of *Z,E* isomers, **1c** provided the best correlation between calcu-

Table 9. Characterization data for the five lowest energy MMX conformers (**1a–1e**) of **1**.

Conformer	E_{Steric}[a] (kcal/mol)	Symmetry group	Disulfide chirality[b]	C-S-S-C torsional angle (deg)	CH_3-N-C=O torsional angle (deg)		$C\text{-}C_{sp2}\text{-}N$ bond angle (deg)		S-S bond length (Å)
					E	*Z*	*E*	*Z*	
1a (*Z,Z*)	0	C_2	R	−104.2	—	177.2	—	119.3	2.073
					—	177.2	—	119.3	
1b (*Z,Z*)	1.15	C_2	L	94.6	—	171.8	—	119.7	2.073
					—	172.4	—	119.6	
1c (*Z,E*)	2.03	—	L	86.9	1.8	173.1	121.5	120.0	2.070
1d (*Z,E*)	4.10	—	L	87.3	11.1	178.0	120.4	119.4	2.072
1e (*Z,E*)	4.38	—	R	−82.2	0.9	173.0	121.0	119.4	2.070
X-ray (*Z,E*)	—	—	L	85.9	2.9	175.1	120.5	119.2	2.035

[a]Relative steric energy.
[b]R = right-handed chirality; L = left-handed chirality.

Fig. 8. Stick plots of the five lowest MMX energy conformers of **1** (**1a–1e**). The ethylene moiety is located at the front of each conformation and is aligned along the *x*-axis for all plots.

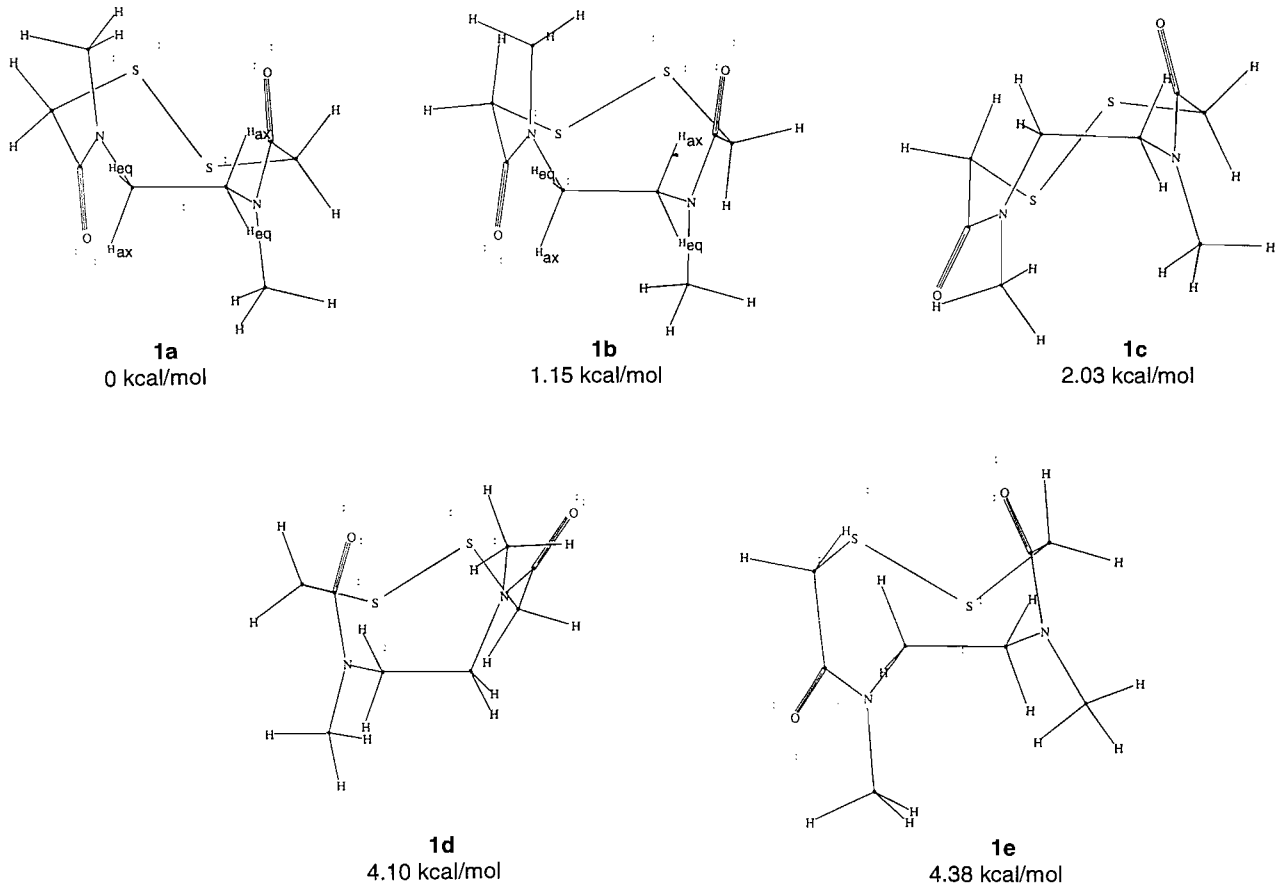

lated and experimental Boltzmann distributions (see Table 3). Moreover, when **1c** was overlapped with the X-ray structure in PCMODEL, it was evident that they were similar (RMS deviation of atoms = 0.037 Å). To achieve a more realistic comparison, conformational changes that might be imposed on **1** by crystal lattice forces were removed from the X-ray structure by subjecting the molecule to the PCMODEL force field energy minimization program. The observed change amounted to approximately 0.6 kcal/mol energy loss upon minimization. The resultant "minimized X-ray" structure was then superimposed on **1c** and **1d** to afford a virtually complete overlay with **1c** (RMS deviation of atoms = 0.021 Å) but gave a poorer alignment with **1d** (RMS deviation of atoms = 0.198 Å). Molecular mechanics had thus accurately predicted the solid

Fig. 9. Ball and stick plots of the MMX-calculated diastereomers **1a** and **1b**, illustrating rotational isomerization about the S—S bond.

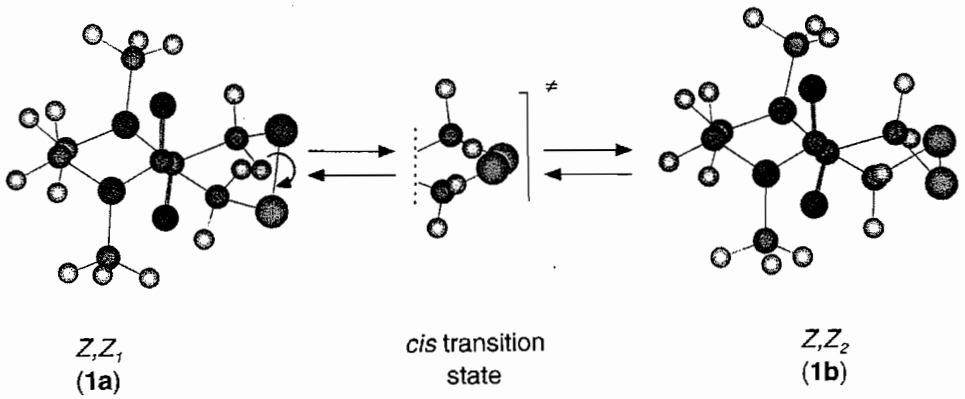

state geometry of the *Z,E* conformer. This fact, coupled with the strong similarities between NOE and computed structural models, suggested that the MM2 force field was a reasonable probe for generating the solution state conformations of **1**. Conformer **1e** is simply the enantiomer of **1c**.

Conformers **1a** and **1b** possess C_2 symmetry and an antiparallel,[7] *Z,Z* configuration with both amide functions essentially coplanar. This antiparallel *Z,Z* arrangement has been reported for other *N*-substituted polyamide heterocycles, including cyclic amides **5** and **6** (23, 24). Steric and electronic factors may account for the configurational preference found in these systems. For example, in the parallel conformation, transannular methyl–methyl contacts and a large internal dipole moment (resulting from the sum of the moments from the parallel C═O groups) will undoubtedly be quite destabilizing.

Analysis of the molecular modelling data and mechanical models led to the conclusion that isomers Z,Z_1 and Z,Z_2 are disulfide ring conformers. At room temperature, interconversion of these rotational isomers was sufficiently slow on the NMR time scale to allow detection by ^{13}C NMR spectroscopy (Table 2). Interconversion occurs presumably through the *cis* transition state by ca. 180° rotation about the asymmetric S—S bond (Fig. 9) and a ^{13}C DNMR study was carried out with the objective of validating the molecular modelling results.

(b) Measurement of the S—S rotational barrier for the $Z,Z_1 \rightleftarrows Z,Z_2$ *equilibrium via* ^{13}C *DNMR*

The simple Arrhenius equation (eq. [2]) was used because previous studies on conformational processes in reasonably inert solvents have shown that $\Delta G^{\ddagger}$ values vary only slightly with temperature (36) and lie within the range of experimental error.

$$[2] \quad k = A \exp(-\Delta G^{\ddagger}/RT)$$

Warming a sample of **1** in DMSO-d_6 from 25.0 to 56.7°C resulted in a temperature-dependent broadening and a subtle high-field migration of the Z,Z_2 N-C_α signal at 45.4 ppm. Rate constants, *k*, for this chemical exchange process were evaluated using the complete bandshape (CBS) method (37). Based on a two-site exchange of the Z,Z_1 and Z,Z_2 N-CH_2 resonances (43.4 and 45.4 ppm, respectively) between 27.0 and 40.2°C, the barrier to $Z,Z_1 \rightleftarrows Z,Z_2$ interconversion ($\Delta G^{\ddagger}$) was measured to be 14.5 ± 1.3 kcal/mol (Table 10). The height of this barrier lies close to the range reported for disulfide rotations in cyclic systems. For example, the barriers to inversion for 1,2-dithiane and 3,3,6,6-tetramethyl-1,2-dithiane have been reported to be 11.6 and 13.6 kcal/mol, respectively (38, 39).

The barrier of 14.5 kcal/mol was too low to be attributed to an amide rotation, particularly one occurring in a cyclic system and, although it was at the high end for reported disulfide rotations, it was reasonable to attribute the $Z,Z_1 \rightleftarrows Z,Z_2$ chemical exchange process to a disulfide rotational mechanism as illustrated in Fig. 9. A large component of the observed barrier is reflected in the energy profile of the acyclic disulfide bond, which has a maximum of ca. 8–10 kcal/mol at a CSSC dihedral angle of 0° (i.e., for the *S-cis* transition state) and a minimum at 90° (40) with the barrier considered to arise from the mutual repulsion between the unshared pairs of 3*pz* nonbonded electrons on adjacent sulfur atoms (41). In cyclic disulfides such as **1**, however, the presence of transannular electrostatic and steric interactions will increase the height of the disulfide rotational barrier. Moreover, the amide groups presumably confer additional rigidity to the ring and likely contribute to the relatively high barrier.

Table 10. Calculated rate constants (from CBS analysis) and Arrhenius parameters for the $Z,Z_1 \rightleftarrows Z,Z_2$ conformational equilibrium.

T (K)	*k* (s^{-1})	1/*T* (K^{-1})	ln *k*
298.5	0.6	0.00335	–0.5108
300.0	0.9	0.00333	–0.1054
302.0	1.0	0.00331	0
304.2	1.2	0.00329	0.1823
306.3	1.2	0.00326	0.1823
309.8	1.8	0.00323	0.5878
311.1	2.2	0.00321	0.7885
313.2	2.4	0.00319	0.8755
317.6	2.7	0.00315	0.9932
329.7	4.6	0.00303	1.5261

[7] The term antiparallel refers to the opposite relative orientation of the amide groups.

It is interesting to note that S—S rotation generated diastereomeric conformations, and not the enantiomers that are commonly observed in acyclic, unsymmetric disulfides (42). The asymmetric nature of the ring introduces a second source of chirality, which, in combination with asymmteric disulfide rotation, confers a diastereomeric relation between the Z,Z_1 and Z,Z_2 stereoisomers.

Unlike the Z,Z_2 isomer, the S-CH_2 protons in the Z,Z_1 structure did not possess pseudoaxial geometry (**1a**, Fig. 8). Analysis of space-filling, mechanical models of the Z,Z_2 structure indicated that a pseudoaxial, S-CH_2 configuration brought one set of lone electron pairs on oppositely related O and S atoms into close proximity. It appeared that the compromised, dipseudoequatorial geometry of the Z,Z_1 conformation defused this transannular interaction by directing the electrons away from each other. Moreover, a pseudoequatorial configuration of S-CH_2 protons was expected to be sterically preferable to a pseudoaxial one as 1,3-diaxial interactions with the methyl groups will destabilize the latter conformation. Some combination of these electronic and steric effects may serve to explain the calculated and observed population distributions between the Z,Z_1 and Z,Z_2 ring conformers (Table 3).

The calculated, MMX conformational energies agreed moderately well with those of the observed populations (Table 3). Since the molecular mechanics calculations mimic isolated molecules in their gaseous state, exact agreement between calculated and experimental populations is unattainable given the present level of computational sophistication. This situation arises from the inability to accurately incorporate solvent effects into the calculations. In addition, certain conformations may be differentially stabilized by solvation (43), particularly in higher energy geometries. In this case, the more energetic, gas-phase *Z,E* (**1c**) conformer will be stabilized to a greater extent than the lower energy Z,Z_2 structure, resulting in a thermodynamic reversal of solution state population levels. The effect may serve to rationalize the differences between calculated and experimental population distributions (Table 3), particularly for the *Z,E* structure.

In analogy to the chemical shift assignments made for protons of the *Z,E* crystal structure (vide supra), the orientation of a MMX-calculated N-CH proton, in relation to its adjacent C=O group, will primarily determine its chemical shift. Consequently, for isomers **1a** and **1b** (Fig. 8), one isochronous N-CH_{ax} pair occupied a pseudoaxial configuration that was essentially *cis* coplanar to the C=O group (i.e., 9.2° and 1.4° removed from the amide plane defined by the atoms O, C, and N) and, therefore, should be the low-field protons at 4.68 and 4.88 ppm, respectively. An interesting confirmation of this pseudoaxial geometry was noted in a ^1H–^1H COSY experiment, where the 4.68 ppm signal was weakly correlated to the N-CH_3 resonance at 3.13 ppm. This was indicative of a stereospecific, four-bond coupling originating from the "W" configuration (44) that is often observed between axial protons α to C-18 or C-19 methyl groups in steroids. Four-bond coupling to the methyl protons was not possible for the pseudoequatorial (H_{eq}) protons in this molecular configuration.

The second, isochronous set of geminal N-CH_{eq} protons in the Z,Z_1 and Z,Z_2 ring isomers occupied pseudoequatorial positions that were approximately 20.9° and 15.6° out of the amide plane. Their respective shifts at 2.64 and 2.71 ppm implied that they were shielded in comparison to the rotationally averaged, *Z,Z* N-CH_2 shift of 3.28 ppm for the open-chain precursor **4** (cf. Table 13). A comparison at a more quantitative level suggests that the H_{eq} protons were shielded by about 0.6 ppm, while the H_{ax} protons were deshielded by 1.5 ppm, respectively. Clearly, the shielding mechanisms (particularly the deshielding forces) at work in the conformational isomers of **1** were quite significant and worthy of further investigation.

Shielding calculations

The objective of this section is to investigate the extent to which it is possible to identify the origins of and to quantify the large N-CH_2 nonequivalences observed in the Z,Z_1 and Z,Z_2 conformers. In addition, we examine the pattern of S-CH_2 nonequivalencies for the *Z,Z* and *Z,E* conformations.

For the purpose of calculating chemical shifts, we have employed a combination of nonlocal density functional theory (DFT) and the guage-independent atomic orbital (GIAO) method using two common ab initio basis sets: Becke3LYP/3-21G* and Becke3LYP/6-31G*. Previous workers have successfully employed a similar level of theory for shift predictions of organic molecules using both DFT (45) and correlated as well as uncorrelated HF (46) methodologies.

*(a) Shift predictions for conformers **1a**, **1b**, and **1c***

The results are presented in Table 11 for the three proton environments as absolute shifts in ppm downfield from TMS. Three primary points derive from the tabulation. First, the calculated shift differences (Δδ) for the eight N-CH_2 and S-CH_2 geminal proton pairs accurately reproduce the measurement with a maximum deviation of 0.2 ppm (cf. Table 1). Second, the absolute shifts from TMS (δ^1H) for the same protons are only slightly less well reproduced, with the majority of deviations from experiment at 0.1–0.2 ppm. The N-CH_3 proton shifts are uniformly overestimated by 0.3–0.5 ppm. However, the calculated values are simple averages over a single N-methyl conformation and are thus subject to the greatest error. The numbers are still quantitatively representative of the spectroscopic outcome. Finally, the economical 3-21G* basis set performs as well as the extended 6-31G* version, both delivering impressive matches with the measured shifts.

(b) Origins of chemical shift differences

The observed chemical shift difference, $\Delta\delta_{OBS}$, between a geminal pair of protons can be broken down heuristically into a number of overlapping effects as depicted by eq. [3] (47).

$$[3] \quad \Delta\delta_{OBS} = \Delta\delta_{MAG} + \Delta\delta_{EL} + \Delta\delta_{SOL} + \Delta\delta_{VDW}$$

The terms $\Delta\delta_{MAG}$, $\Delta\delta_{EL}$, $\Delta\delta_{SOL}$, and $\Delta\delta_{VDW}$ refer to the *net* chemical shift between N-CH_2 or S-CH_2 protons ascribed to shielding contributions from magnetic anisotropy, electric field, solvent, and van der Waals effects of all neighbouring groups in the molecule.

The $\Delta\delta_{MAG}$ and $\Delta\delta_{EL}$ contributions arise from the perturbation of a proton by the magnetic field and electric dipoles of polar groups such as amide functionalities by an obtained through-space mechanism. Rough estimates can be estimated by applying modified forms of McConnell's (48) and Buckingham's (49) equations, respectively. The polar character of the amide group can also contribute to $\Delta\delta_{OBS}$ through the polarization of the solvent via a reaction field. However, this

Table 11. Becke3LYP/GIAO ^{1}H NMR chemical shift (ppm) predictions for MMX optimized disulfide conformers **1a**, **1b**, and **1c** with the 3-21G* and 6-31G* basis sets.[a,b]

	Conformer					
	Z,Z$_1$		Z,E		Z,Z$_2$	
Signal	δ^1H	$\Delta\delta$	δ^1H	$\Delta\delta$	δ^1H	$\Delta\delta$
N-CH$_2$						
3-21G*	2.6(0.0)	2.0(0.0)	3.1(0.1)	1.2(0.1)	2.7(0.0)	2.3(0.1)
	4.6(0.1)		4.3(0.0)		5.0(0.1)	
			3.3(0.2)	1.0(0.2)		
			4.3(0.0)			
6-31G*	2.7(0.1)	1.9(0.1)	3.1(0.1)	1.3(0.0)	2.8(0.1)	2.2(0.0)
	4.6(0.1)		4.4(0.1)		5.0(0.2)	
			3.2(0.1)	1.2(0.0)		
			4.4(0.1)			
S-CH$_2$						
3-21G*	3.1(0.3)	0.0(0.0)	3.4(0.2)	0.6(0.2)	3.3(0.1)	0.5(0.2)
	3.1(0.4)		4.0(0.0)		3.8(0.1)	
			3.1(0.1)	0.9(0.2)		
			4.0(0.2)			
6-31G*	3.2(0.2)	0.2(0.2)	3.5(0.1)	0.5(0.1)	3.2(0.0)	0.6(0.1)
	3.4(0.1)		4.0(0.0)		3.8(0.1)	
			3.0(0.0)	1.0(0.1)		
			4.0(0.2)			
N-CH$_3$[c]						
3-21G*	3.5(0.4)		3.4(0.4)		3.5(0.3)	
			3.7(0.5)			
6-31G*	3.5(0.4)		3.4(0.4)		3.6(0.4)	
			3.7(0.5)			

[a]Relative to TMS at the same basis set with MP2/6-31G* optimized geometry; isotropic ^{1}H shifts: 3-21G* 32.9 ppm; 6-31G* 32.3 ppm.

[b]Parenthetical values are the absolute chemical shift differences in ppm between the measured (Table 1) and calculated values.

[c]Tabulated chemical shifts are simple averages for the three methyl protons.

shift contribution from the solvent ($\Delta\delta_{SOL}$) was demonstrated by Clayden and Williams to be unimportant in determining the methylene nonequivalence in cyclotetrasarcosyl, **5** (50). The absence of exchangeable protons and a concentration dependence for the magnitude of the N-C*H*$_2$ shift difference in **1** indicates that specific solvent–solute and (or) solute–solute interactions are not likely shift factors either.

The expression $\Delta\delta_{VDW}$ reflects the operation of shielding effects when hydrogen atoms are subject to intramolecular steric or van der Waals interactions with proximate nuclei (51). Qualitatively, the direction of shielding can be associated with the net nuclear charge on the resonant proton, which, in turn, depends on the predominance of either an attractive or repulsive interaction. For example, if the resonant proton feels an *attractive* van der Waals interaction with a proximate group, its effective nuclear charge will be increased, resulting in an *upfield* shift (shielding) of the hydrogen nucleus. Conversely, in the *repulsive* van der Waals regime, electrostatic repulsion of interacting electron clouds will induce charge polarization in the H→C bond direction and will produce a *downfield* shift (deshielding) of the resonant proton (52). In general, intramolecular separations at, or smaller than, the sum of the van der Waals radii of the interacting groups usually result in repulsive van der Waals interactions, while attractive interactions will dominate at slightly larger interatomic distances. The attractive interaction is relatively weak compared to its stronger repulsive counterpart, so deshielding effects are generally much larger and more common than the shielding ones (53). Instances of such deshieldings have been observed mostly in rigid systems, where one or more hydrogen atoms is forced too close to other groups because of rigid geometrical constraints (51). For example, the magnitude of the δ_{VDW} shift and N-C*H*$_2$ nonequivalence in a series of hindered amides has been linearly correlated to the size and number of the interacting groups (54).

In contrast to **5** (50), a $\Delta\delta_{VDW}$ contribution to $\Delta\delta_{OBS}$ cannot be ruled out for **1** since van der Waals contacts involving the downfield H_{ax} protons were detected in the calculated MMX

Fig. 10. Space-filling models of **1b** from (*a*) side and (*b*) top perspectives. Note the van der Waals compression of the S-CH pseudoaxial proton with the N-CH_3 protons, and the carbonyl oxygen with H_{ax}. The N-CH_3 group has been rotated by ca. 60° to illustrate steric compression.

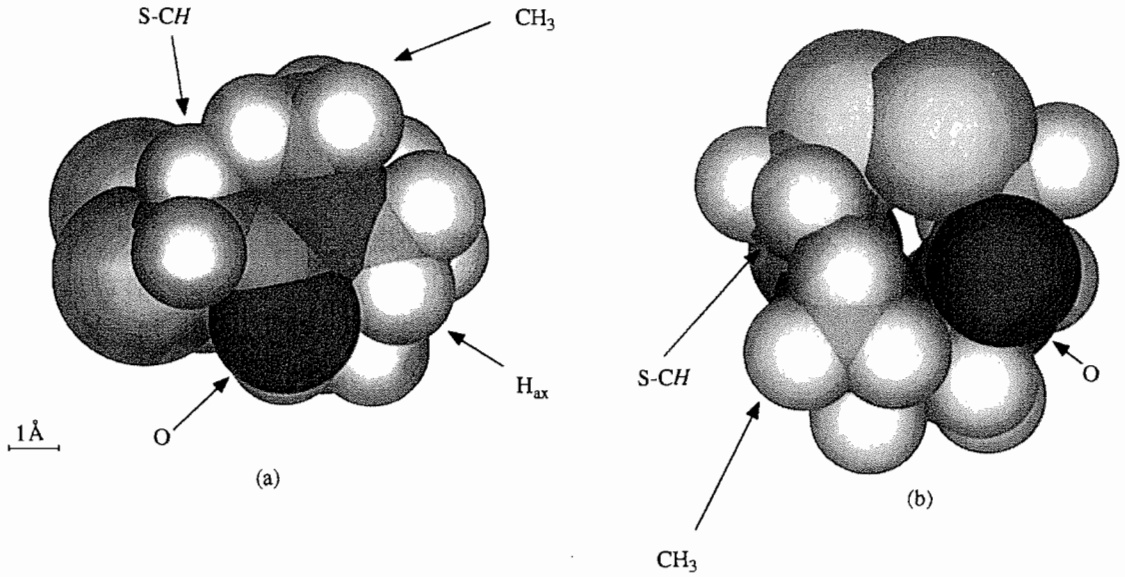

and crystal structures. An example of these through-space contacts is illustrated for the Z,Z_2 conformer (Fig. 10). CPK space-filling representations are used to illustrate an "effective size" for each atomic electron cloud based on their characteristic van der Waals radii (r_{VDW}). Intra-atomic measurements showed that the oxygen (r_{VDW} = 1.5 Å) (34) and methyl (r_{VDW} = 2.0 Å) groups protrude into the electron cloud of the H_{ax} (r_{VDW} = 1.2 Å) protons by at least 0.2 and 0.1 Å, respectively. Thus, a downfield shift is predicted for the H_{ax} protons. In contrast, the H_{eq} protons are not expected to be influenced by a paramagnetic van der Waals shift given its sterically unencumbered, pseudoequatorial geometry. A quantitative assessment of the $\Delta\delta_{VDW}$ contributions to methylene shift nonequivalences was provided by ab initio shift calculations (vide infra).

(c) The N-CH_2 protons

Our strategy for deconvoluting the various intramolecular influences on the differential chemical shifts of geminal protons is to carve the molecule into smaller fragments of identical structural geometries and to compute the corresponding chemical shifts using the ab initio methodology employed for the whole molecule (Table 11). Consequently, seven substructures were prepared (see Experimental) and subjected to a DFT/GIAO evaluation for comparison with **1a-1c** (Table 12). The following analysis shows that the observed shieldings are a complex blend arising from the amide dipole, N–CH steric effects, and, in the case of S-CH_2 protons, the sulfur lone pairs.

Consider the 2.0 ppm difference between the geminal pseudoaxial and equatorial N-CH_2 protons in **1a** (Z,Z_1). A comparison of 1,2-diaminoethane, ((OHCN-CH_2)$_2$ and N-demethyl **1a** with the corresponding N-methyl structures (Table 12) demonstrates that methylation causes the geminal proton *syn* to the methyl group (H_{syn}) to shift upfield by 0.3–0.5 ppm. By contrast, H_{anti} is deshielded by 0.1–0.3 ppm upon methyl addition. The resulting difference is around 0.6 ppm. Further addition of the CHO unit induces a small deshielding of −0.1 to −0.2 for H_{syn}, but a much larger deshielding of −1.5 to −1.8 ppm results for H_{anti}. Overall, H_{syn} experiences an approximate 0.2–0.3 ppm upfield shift (relative to the protons in diaminoethane) largely as a result of an attractive van der Waals interaction with the N-methyl group. H_{anti}, on the other hand, is pulled 1.8 ppm downfield mainly by dipolar effects of the amide group, but supplemented by a small δ_{VDW} contribution from N-methyl contact. The net geminal proton separation is 2.0–2.1 ppm, as observed and predicted for **1a** (Table 11).

Precisely the same situation applies to the minor conformation **1b** (Z,Z_2). Here, the observed geminal splitting of 2.2 ppm is due to the effect of amide group deshielding (ca. 1.8–2.0 ppm) with a diminutive contribution of 0.3 ppm from steric interaction with the N-CH_3 group. The axial H_{anti} is somewhat nearer the C═O oxygen in **1b** than **1a** (2.41 vs. 2.44 Å, respectively), while the C═O and C—H bonds are closer to a common plane (ϕ(H—C---C═O) = 12.3° and 24.5°, respectively).

A similar analysis for the third conformer, **1c** (Z,E), shows that the presence or absence of the N-methyl function has little effect on the N-CH_2 shift difference (≤0.1 ppm, Table 12). The *trans* and *cis* amide groups contribute the most, providing 1.0 and 1.2 ppm, respectively, to the observed geminal splitting. On the *trans* half of the molecule, the axial N-CH_2 ($H_{anti,1}$) is situated 2.54 Å from the amide oxygen and twisted out of the H—C---C═O plane by 39°. Both factors cause a reduction in the geminal split relative to **1a** and **1b**, which is 1.1 ppm based on the fragment analysis (Table 12). On the *cis* side, the axial N-CH_2 proton ($H_{anti,2}$) is too far from the adjacent C═O to significantly experience any electronic effects, but lies only 2.7 Å cross-ring from the oxygen of the *trans* amide. A more revealing description of its location sites the proton 1.74 Å *above* the plane of the *trans* amide but shifted 2.01 Å away from the carbonyl oxygen (Fig. 11). This is to be compared with $H_{anti,1}$,

Table 12. Becke3LYP/GIAO ^{1}H NMR geminal X-CH_2 chemical shift (ppm) predictions for MMX optimized disulfide conformers **1a**, **1b**, and **1c** and capped fragments with the 3-21G* and 6-31G* basis sets.[a,b,c]

	Conformer								
	Z,Z_1 3-21G* (6-31G*)			Z,E[d] 3-21G* (6-31G*)			Z,Z_2 3-21G* (6-31G*)		
Signal	H_{syn}	H_{anti}	Δδ	H_{syn}	H_{anti}	Δδ	H_{syn}	H_{anti}	Δδ
1 (N-CH_2)	2.6(2.7)	4.6(4.6)	2.0(1.9)	3.3(3.2)	4.3(4.4)	1.0(1.2)	2.7(2.8)	5.0(5.0)	2.3(2.2)
				3.1(3.1)	4.3(4.4)	1.2(1.3)			
(H_2N-CH_2)$_2$	2.9(3.0)	2.9(2.9)	0.1(0.0)	2.8(2.8)	3.0(3.2)	0.2(0.4)	2.9(3.1)	2.7(2.8)	0.2(0.3)
				3.0(3.1)	2.7(2.9)	0.3(0.2)			
(MeHN-CH_2)$_2$	2.4(2.6)	3.2(3.2)	0.8(0.6)	2.9(3.0)	3.1(3.3)	0.2(0.3)	2.4(2.6)	3.2(3.2)	0.8(0.6)
				2.7(2.8)	2.7(2.9)	0.0(0.1)			
(OHCNH-CH_2)$_2$	3.0(2.9)	4.7(4.7)	1.7(1.8)	3.1(2.8)	4.3(4.3)	1.2(1.5)	3.0(2.9)	4.9(4.8)	1.9(1.9)
				3.2(3.1)	4.3(4.3)	1.1(1.2)			
MeHN-CH_2-	2.8(2.2)	3.2(2.6)	0.4(0.4)	3.1(3.1)	3.5(3.6)	1.1(1.1)	2.7(2.9)	3.2(3.1)	0.5(0.2)
CH_2-NMeCHO	2.4(2.4)	4.7(4.7)	2.3(2.3)	3.1(3.0)	3.3(3.4)	1.1(1.1)	2.4(2.4)	4.8(4.8)	2.4(2.4)
				3.0(2.8)	4.1(3.9)	0.4(0.5)			
				2.7(3.0)	3.8(4.1)	0.2(0.4)			
(OHCNMe-CH_2)$_2$	2.6(2.6)	4.7(4.7)	2.1(2.1)	3.1(3.0)	4.3(4.4)	1.2(1.8)	2.6(2.6)	4.9(4.8)	2.3(2.2)
				3.0(3.0)	4.2(4.3)	1.2(1.3)			
1 (NH/N-CH_2)[e]	3.0(3.0)	4.4(4.5)	1.4(1.5)	3.1(3.0)	4.1(4.2)	1.0(1.2)	3.0(3.0)	4.7(4.8)	1.7(1.8)
				3.2(3.2)	4.2(4.3)	1.0(1.1)			
1 (S-CH_2)	3.1(3.2)	3.1(3.4)	0.0(0.2)	4.0(4.0)	3.1(3.0)	0.9(1.0)	3.8(3.8)	3.3(3.2)	0.5(0.6)
				4.0(4.0)	3.4(3.5)	0.6(0.5)			
HCH_2-S-S-CH_2H	2.1(2.2)	2.9(3.0)	0.8(0.8)	2.7(2.9)	2.2(2.2)	0.5(0.7)	2.4(2.6)	2.3(2.4)	0.1(0.2)
				3.1(3.2)	2.0(2.2)	1.1(1.0)			
1 (NH/S-CH_2)[e]	2.7(2.8)	3.2(3.5)	0.5(0.7)	3.0(3.0)	3.4(3.3)	0.4(0.3)	2.8(2.9)	3.5(3.4)	0.7(0.5)
				4.0(4.0)	3.3(3.3)	0.7(0.7)			

[a]H_{syn} is the CH_2 proton *syn* to CH_3 or H of the N-R group; H_{anti} is defined similarly. The shift values are given in ppm relative to TMS; cf. footnote *a*, Table 1.

[b]Parenthetical values are those calculated from the 6-31G* basis set.

[c]Δδ is the chemical shift difference between NCH_2 and SCH_2 geminal protons in ppm.

[d]*trans*-Amide values are listed first; *cis*-amide, second.

[e]Bis-*N*-demethyl **1**.

which is 0.70 Å *below* the *trans* amide plane and likewise shifted from the carbonyl oxygen by 2.47 Å.

Qualitatively, we can predict that both $H_{anti,1}$ and $H_{anti,2}$ are deshielded relative to their geminal partners because of their positions inside the deshielding space of the *trans* C=O shielding cone. Their observed shifts and splittings are accurately reproduced by the shift calculations (Table 11) and confirmed to be primarily a deshielding effect of the (*trans*) amide (Table 12) by the fragment shielding treatment. The latter analysis suggests a geminal separation of 1.3 ppm (H_{anti}: (H_2N-CH_2)$_2$ vs. (OHCNH-CH_2)$_2$, Table 12), in agreement with experiment.

(d) The S-CH_2 protons

The observed splittings for the geminal protons α to sulfur are considerably less than those α to nitrogen (Table 1). Superficially, one might conclude that the local "magnetic" environments are therefore similar. On the other hand, there is no obvious intuitive reason for drawing this inference based on molecular geometry. Both the N-CH_2 and S-CH_2 sites are equally asymmetric: a pseudoaxial and a pseudoequatorial proton residing at each center. Magnetic similarity must then arise from the near cancellation of effects. To accomplish the analysis, we examine chemical shifts in the S-CH_2 moieties of **1**, N-demethyl **1**, and the dimethyldisulfide fragment given in Table 12.

The abundant conformer **1a** (Z,Z_1) exhibits its S-CH_2 protons as magnetically equivalent (Tables 1 and 11). Yet, the dimethyldisulfide fragment reveals a 0.8 ppm difference between geminal protons (Table 12). This surprisingly large isochrony can be appreciated by recognizing that H_{anti} resides almost directly above the S—S bond and is consequently deshielded by both lone pairs on the adjacent sulfur (Fig. 8, **1a**). From MeSSMe to **1a**, H_{syn} experiences a 1.0 ppm downfield shift as a result of its position close to the amide plane and its steric interaction with the N-methyl group, the latter repulsive van der Waal contact contributing 0.4 ppm. H_{anti} is simultaneously deshielded by only 0.2 ppm, derived entirely from dipolar interaction with the amide. The net result is that both protons experience almost identical shifts, although each is influenced significantly and dissimilarly by the S—S, (N)Me, and amide moieties. A parallel analysis can also serve

Fig. 11. A ball and stick plot of the MMX diamide **1c**, showing the H_{syn} and H_{anti} positions relative to the *trans* carbonyl oxygen. Numerical values correspond to distances in Å.

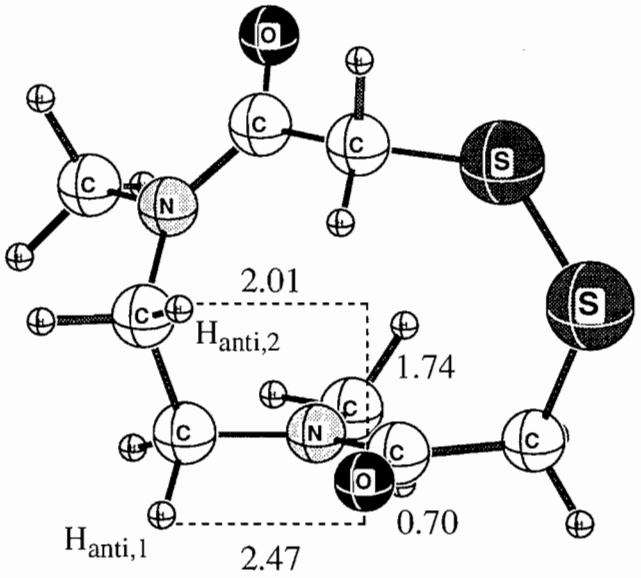

to rationalize the S-CH_2 $\Delta\delta_{OBS}$ for **1b** (Z,Z_2). However, the shielding forces affecting H_{syn} and H_{anti} are greater (owing to their stricter pseudoaxial and pseudoequatorial geometries) and are manifest as a larger, geminal shift difference of 0.7 ppm (Table 1).

Conformer **1c** (*Z,E*) exhibits $\Delta\delta$'s of similar magnitude for protons α to N and S around the *trans*-amide functionality. While they arise from alternative factors, a decomposition analysis from values in Table 12 provides a quantitative assessment. Noteworthy is the situation for the geminal hydrogen pair adjacent to the *cis*-amide center, which sustains a rather small observed isochrony of 0.4 ppm (Table 1). The C—H bond containing H_{anti} is nearly eclipsed with the S—S bond (ϕ = 12.0°), while the same bond involves an unusually short, H---H van der Waals contact (1.97 Å) with a *cis*-disposed H_{anti} of the adjacent N-CH_2 group (respectively, H(3b) and H(6b), Fig. 5 inset). The combination promotes a 1.4 ppm deshielding that is matched by a nearly identical H_{syn} deshielding of 0.9 ppm from the *cis*-amide moiety (cf. MeSSMe and **1**, Table 12). Once again, large and compensatory effects lead to a diminutive geminal $\Delta\delta$.

Experimental

Materials

Acetonitrile was distilled from P_2O_5 and the distillate was redistilled from CaH_2, discarding the first 5 and the last 10%. Ethanol (EtOH) was dried and purified via distillation from magnesium turnings and stored over freshly activated 4 Å molecular sieves. All chemicals were purchased from Aldrich Chemical Company (Milwaukee, Wis.).

Melting points (mp) were recorded on a Gallenkamp capillary tube melting point apparatus and are uncorrected.

Analytical thin-layer chromatography (TLC) and column chromatography (according to the "flash" method of Still et al. (55)) were carried out on E. Merck silica gel 60 F_{254} coated Al plates of 0.2 mm thickness and 0.040–0.063 mm (230–400 mesh), respectively. TLC visualization was achieved using a combination of either a UV lamp at 254 nm or I_2 vapour and treatment with a phosphomolybdic acid spray (20 g of phosphomolybdic acid hydrate and 15 g $Ce(SO_4)_2$ dissolved in 1 L of 10% H_2SO_4) followed by heating to ca. 130°C.

Electrospray (ES) mass spectrometry (MS) was performed on a Fisons VG Platform LC–MS electrospray mass spectrometer. Other mass spectra were obtained on a VG ZAB-E mass spectrometer with sample introduction via a direct inlet system. Infrared spectra (IR) were recorded on a Perkin–Elmer 283 spectrometer using either liquid cells with methylene chloride or chloroform as solvents or potassium bromide pellets. The abbreviations (s) = strong, (m) = medium, and (w) = weak are used to describe the intensity of particular bands in the IR spectra.

X-ray diffraction

$C_8H_{14}N_2O_2S_2$ fw = 234.3

Triclinic, a = 7.0570(10), b = 8.071(2), c = 11.012(2) Å, α = 106.05(2)°, β = 93.41(1)°, γ = 114.93(1)°, V = 535.3(3) $Å^3$, Z = 2, ρ_c = 1.454 g cm^{-3}, μ = 4.342 mm^{-1} (23°C; CuKα_1, λ = 1.54178 Å)

Crystals of **1** were grown by very slow recrystallization from freshly distilled tetrahydrofuran at −15°C. A colorless plate having approximate dimensions of 0.20 × 0.05 × 0.15 mm was mounted on a glass fiber. All measurements were made on a Rigaku AFC6R diffractometer with graphite-monochromated CuKα radiation and a rotating anode generator.

Cell constants and an orientation matrix for data collection were obtained from a least-squares refinement using the setting angles of 24 carefully centered reflections in the range 7.0 < 2θ < 45.0°. Based on packing considerations, a statistical analysis of intensity distribution and the successful solution and refinement of the structure, the space group was determined to be $P\bar{1}$ (no. 2).

The data were collected at a temperature of 23 ± 1°C using the ω–2θ scan technique to a maximum 2θ value of 110.1°. Scans of (1.21 + 0.30 tan θ)° were made at a speed of 32.0°/min (in ω). The weak reflections ($I < 10.0\sigma_I$) were rescanned (maximum of nine rescans) and the counts were accumulated to assure good counting statistics. Stationary background counts were recorded on each side of the reflection. The ratio of peak counting time to background counting time was 2:1. The diameter of the incident beam collimator was 0.5 mm and the crystal-to-detector distance was 400.0 mm.

Of the 1479 reflections that were collected, 1362 were unique (R_{int} = 0.032). The intensities of three representative reflections, which were measured after every 150 reflections, remained constant throughout data collection, indicating crystal and electronic stability (no decay correction was applied). The data were corrected for Lorentz and polarization effects.

The structure was solved by direct methods. All non-hydrogen atoms were refined with anisotropic thermal parameters. Hydrogen atoms were placed geometrically and not refined. A correction was made for extinction (χ = 0.005(3) where $F^* = F[1 + 0.002\chi F^2/\sin 2\theta]^{-1/4}$) and an absorption correction was applied using the program DIFABS (56), employing transmission factors ranging from 0.69 to 1.20. Atomic scattering fac-

tors for all atoms and corrections for anomalous dispersion for C, O, N, and S were taken from the International Tables for Crystallography, Vol. C (57). Refinement minimized the function $\Sigma\omega(|F_o| - |F_c|)^2$, with $\omega = (\sigma^2F + 0.0008F^2)^{-1}$. The final solution, with $R = 4.67\%$ ($R = \Sigma(||F_o| - |F_c||)\Sigma F_o$) and $\omega R = 6.80\%$ for 1006 reflections ($I > 2\sigma_I$), showed no significant peaks in the final difference map. The goodness-of-fit was $S = 1.51$. The program SHELXTL PC was used for all calculations (58).[8]

NMR spectroscopy

Proton nuclear magnetic resonance (^{1}H NMR) spectra were recorded on Varian EM 390, Bruker MSL-100, AC-200, WM-250, or AM-500 spectrometers, with the majority of experiments acquired at 500.135 MHz on the latter instrument using a 5 mm dual-frequency ^{1}H–^{13}C probe. Spectra were obtained in eight scans in 16K data points over a 5.000 kHz spectral width (1.638 s acquisition time). Sample temperature was maintained at 303 K by a Bruker BVT-1000 variable temperature unit. The free induction decay (FID) was processed using exponential multiplication (line broading: 0.2 Hz) and was zero-filled to 32K before Fourier transformation. The abbreviations s = singlet, d = doublet, t = triplet, q = quartet and m = multiplet refer to the multiplicities of the signals observed.

Broad band decoupled, natural abundance carbon-13 nuclear magnetic resonance (^{13}C NMR) spectra were recorded on a Bruker AM-500 spectrometer at 125.759 MHz using the 5 mm dual frequency ^{1}H–^{13}C probe, except in one experiment, which was acquired on a Bruker WP-80 instrument at 20.115 MHz. The spectra were acquired over a 30.0 kHz spectral width in 16K data points (0.279 s acquisition time). The ^{13}C pulse width was 2.5 μs (35° flip angle). A 0.5 s relaxation delay was used. For spectral editing, the standard *J*-modulated spin-sort pulse sequence was used, incorporating a 7.3 μs ^{13}C 90° pulse width and a relaxation delay of 2.5 s. The FIDs were processed using exponential multiplication (line broading: 3.5 Hz) and zero-filled to 32K before Fourier transformation.

NOE difference spectra were obtained by subtraction of the off-resonance control FID from the on-resonance FID under non-spinning conditions and employing a sweep rate of 19 Hz. The signal of interest was selectively saturated for 5 s and the decoupler was gated off during acquisition. This saturation period also served as the relaxation delay. Normally, eight scans were acquired for each irradiation with the cycle of irradiation repeated 10 times. Free induction decays were processed using exponential multiplication with a line broadening of 4.0 Hz before Fourier transformation. The sample was not degassed, so the enhancements are not quantitative.

The ^{13}C–^{1}H 2-D chemical shift correlation spectrum was acquired using the standard pulse sequence incorporating the BIRD pulse during the evolution period for the ^{1}H–^{1}H decoupling in F_1 (59–61). The spectra in F_2 were recorded over a spectral width of 3.76 kHz in 4K data points. The 256 FIDs in F_1 were obtained over a ^{1}H spectral width of 1.52 kHz. Each FID was acquired in 200 scans. The fixed delays in the pulse sequence were a 1.0 s relaxation delay, BIRD pulse and polarization transfer delays ($1/2\ ^1J_{CH}$) of 0.003 571 s, and a refocussing delay ($1/4\ ^1J_{CH}$) of 0.001 786 s. The ^{13}C 90° pulse width was 6.4 μs while the ^{1}H 90° pulse width through the decoupler channel was 18.6 μs. The data were processed using exponential multiplication (line broadening: 5.0 Hz) in F_2 and unshifted sine bell in F_1. Zero-filling in F_1 resulted in a 2048 × 1024 data matrix.

^{13}C DNMR spectra were recorded over a 2.066 kHz spectral width in 8K data points (1.98 s acquisition time) incorporating a 5.5 μs pulse width and a 9.0 s relaxation delay to optimize sensitivity and digital resolution. The sample and probe were allowed a 10 min equilibration period per 5°C increment. An external digital thermocouple was used to measure the probe temperature to an accuracy of ±0.5°C. Rate constants were estimated by visual fitting of experimental to computer-simulated spectra measured for a given temperature. The calculated spectra were generated on an IBM PS/2 model 30 (286) microcomputer equipped with a HP 7550A graphics plotter using the simulation program EXCHANGE (available from R.E.D. McClung, Department of Chemistry, University of Alberta, Edmonton, AB T6G 2G2, Canada). The intrinsic linewidth of 0.35 Hz was obtained from a measurement of the peak width at one-half peak height of the S-CH_2 resonance at 35.61 ppm at 25.5°C. The $\Delta G^{\ddagger}$ for disulfide rotation was calculated from the slope of the regression line derived from an Arrhenius plot of ln *k* versus $1/T$ in Quattro Pro (3.01). The data points corresponding to T = 298.5, 317.6, and 329.7 K were omitted from the regression analysis. The error in $\Delta G^{\ddagger}$ was measured by the standard deviation of the regression coefficient. The theoretical line was drawn by fitting the $1/T$ data series to the regression equation.

The solid state, CP-MAS ^{13}C spectrum was obtained at 25.18 MHz on a Bruker MSL-100 spectrometer operating at 2.35 T using a **1** ms contact time and a recycle time of 10 s. Crystals of **1** (0.10 g), obtained by slow evaporation of a THF solution of the compound, were pulverized and diluted with KBr prior to analysis.

The compounds analyzed via NMR were dissolved in either deuterated acetone, deuterated benzene, deuterochloroform, or deuterated dimethyl sulfoxide (CD_3COCD_3, C_6D_6, $CDCl_3$, or DMSO-d_6, respectively) obtained from MSD Isotopes. ^{1}H and ^{13}C chemical shifts are reported in parts per million (ppm) using either TMS (0.0 ppm) as an internal reference or the residual signal of the following solvents: CD_3COCD_3 (2.04; 29.8 ppm), C_6D_6 (7.15; 128.0 ppm), $CDCl_3$ (7.26; 77.0 ppm), and DMSO-d_6 (2.49; 39.5 ppm).

Molecular mechanics calculations

Steric energies and conformations were calculated and minimized in PCMODEL V4.0 (available from K. Gilbert, Serena Software, Box 3076, Bloomington, IN 47402-3076, U.S.A.) using the MMX force field derived from the MM2 force field of N.L. Allinger (available from Quantum Chemistry Pro-gram Exchange, Chemistry Department, Indiana University, Bloomington, IN 47405, U.S.A.). The calculations were performed on an IBM PS/2 model 70 (486) microcomputer. The MMX force field includes the parameters necessary for the minimization calculations. Calculated steric energies were reported relative to the global minimum structure. Vicinal coupling constants

[8] Tables of observed and calculated structure factor amplitudes and atomic coordinates (ref.: R.B.M. Ph.D. Dissertation, McMaster University; data deposited in 1992 on 5 $\frac{1}{4}$ in. floppy diskette) may be purchased from: The Depository of Unpublished Data, Document Delivery, CISTI, National Research Council Canada, Ottawa, Canada K1A 0S2.

Table 13. ^{1}H NMR (500 MHz) characterization of **4** in $CDCl_3$ at 303 K.

	Conformer		
Signal	*Z,Z*	*Z,E* ppm (multiplicity, integral[a])	*E,E*
N-CH_3	2.60(s,6H)	2.42(s,3H) 2.71(s,3H)	2.52(s,6H)
S-CH_2	2.79(s,4H)	2.77(s,2H) 2.84(s,2H)	2.72(s,4H)
(N-CH_2)$_2$	3.28(s,4H)	3.08(t,2H) 3.16(t,2H)	2.93(s,4H)
Aromatic		7.14–7.38(m,32H[b])	

[a]Integrals are relative within a geometrical isomer.
[b]Overlapping residual $CHCl_3$.

Table 14. ^{13}C NMR (126 MHz), *J*-modulated characterization of **4** in $CDCl_3$ at 303 K.

	Conformer					
Signal	*Z,Z*	*Z,E* ppm (relative intensity)	*E,E*	*Z,Z/Z,E*	*Z,Z/E,E*	*Z,E/E,E*
N-CH_3	35.98(–52)	34.02(–10) 36.67(–10)	—	2.6	—	—
S-CH_2	35.10(55)	34.64(11) 34.83(11)	33.88(5)	2.5	11.0	4.4
(N-CH_2)$_2$	44.76(52)	46.94(11) 47.53(11)	—	2.4	—	—
Aromatic	126.64–129.73, 143.80(4), 143.92(17), 144.00(18), 144.05(18)					
C-Tr	66.71(11)	66.81(3.03) 66.94(2.74)				
CO-NH	168.77(26)	168.24(6) 168.52(7)				

measured from energy-minimized structures were calculated using the Altona modification of the Karplus equation, which takes into account substituent electronegativity (62).

To ensure a comprehensive search of conformational space, initial geometries were generated by either systematic or random methods (63). Systematic geometry searches were typically conducted by merging all combinations of accepted ground state geometries of the disulfide, amide, and ethyl functional groups of **1**; i.e., 90° torsional angle for the disulfide linkage, 180° (*trans*) and (or) 0° (*cis*) torsional angles for the amide groups, and a staggered configuration for the ethyl fragment. Random geometries were typically generated by either random or pseudorandom atomic variations on either minimized structures or two-dimensionally drawn images. After a crude starting geometry was produced, it was allowed to relax into an optimized geometry by the MMX force field. The search was terminated when new minima within 5 kcal/mol of the global minimum ceased be to found. Starting geometries were preminimized without hydrogen atoms and then reminimized with added hydrogens. This procedure avoids forcing hydrogens and lone electron pairs into high-energy configurations (64). Minimized structures were finally reminimized to ensure full convergence.

Shielding calculations

As a preliminary, the MMX optimized structures of **1a**, **1b**, and **1c** were modified by structural fragmentation. For example, the full structures were converted from N-CH_3 to N-H by eliminating the methyl protons and replacing the carbon by hydrogen with an N—H bond. Similarly, the other cut-down structures were generated from the three key conformations by retaining the MMX geometry, but eliminating various fragments. Heavy-atom replacements were made by hydrogen. The resulting N—H and C—H bond length were assigned values of 1.00 and 1.10 Å, respectively, but no additional changes to molecular geometry were made. The series of structures generated are listed in Tables 11 and 12. To obtain absolute chemical shifts, the structure of tetramethylsilane (TMS) was optimized with the MP2(Full)/6-31G* protocol to give r(Si—C) = 1.884 Å, r(C—H) = 1.094 Å, θ(Si-C-H) = 111.3° and θ(C-Si-C) = 109.47°.

All chemical shift evaluations were performed as single-point calculations on the original and modified structures using the Gaussian-94 series of programs (65). Becke's nonlocal density functional theory (DFT) (66, 67) was combined with two standard basis sets to generate the wave functions, Becke3LYP/3-31G* and Becke3LYP/6-31G*. Each calcula-

tion was followed with a Gauge-Independent Atomic Orbital (GIAO) (68) evaluation. The resulting isotropic magnetic shieldings are presented in Tables 11 and 12.

2-(Triphenylmethyl)thioacetic acid (2)

This synthesis was performed according to the method of Brenner et al. (12). A solution of triphenylmethanol (48.0 g, 184.0 mmol), mercaptoacetic acid (12.2 mL, 184.0 mmol), and glacial acetic acid (160 mL) was heated to 70°C. Boron trifluoride etherate (32.0 mL) was added and the resulting brown solution was stirred at room temperature for 50 min. The reaction mixture was poured into ice-cold distilled water, depositing a clear oil that solidified over 18 h at 5°C. The solid was broken and washed with distilled water, then with a small amount of diethyl ether, and was dried in vacuo to give a white solid (40.0 g, 65%). A further crop (4.3 g, 7%) was recovered from the ether washings and purified by recrystallization from toluene; mp 155.0–157.0°C (lit. (6, 12) mp 158.5–160.0°C).

***N*-Succinimido 2-(triphenylmethylthio) acetate (3)**

This synthesis was performed according to the method of Brenner et al. (12). To an ice-cooled solution of acid **2** (5.01 g, 15.00 mmol) and *N*-hydroxysuccinimide (1.72 g, 15.00 mmol) in DME (38 mL) was added DCC (3.20 g, 1.1 equiv., 15.5 mmol) such that the temperature remained at approximately 0°C. The resulting mixture was then stored at 5°C for 18 h and then filtered and washed with ice-cold CH_2Cl_2. The filtered, white crystalline solid (DCU) was collected and discarded. The combined CH_2Cl_2 filtrate and washings were pooled and concentrated in vacuo to afford a white solid. Residual amounts of DCU were removed via recrystallization from ethyl acetate to give large, opaque prisms (5.43 g, 84%); mp 178.5–180.0°C (lit. (6, 12) 178.5–179.5°C).

***N,N′*-{Dimethyl-bis[2-(triphenylmethyl)thioacetyl]}-ethylenediamine (4)**

To a stirred solution of the succinimidoyl ester **3** (1.00 g, 2.32 mmol) in acetonitrile (10 mL) was added a solution of *N,N′*-dimethylethylenediamine (120 μL, 1.1 mmol) in AN (1 mL) and NEt_3 (2 drops) under a N_2 atmosphere. After 12 h, the milky-white suspension was concentrated to 2 mL, diluted with 0.5 N HCl (100 mL), and extracted with CH_2Cl_2 (200 mL). The organic layer was backwashed with 0.5 N HCl (200 mL), with 0.5 N $NaHCO_3$ (200 mL), and dried over $MgSO_4$ for 1 h. Filtration and concentration of the filtrate in vacuo afforded a white solid (621 mg, 76%). Chromatographic purification of the resultant crude (stepwise elution: 100% CH_2Cl_2 followed by 2% MeOH in CH_2Cl_2) gave a white solid; mp 71.0–72.5°C; R_f 0.79 (10% MeOH in CH_2Cl_2); IR(KBr pellet): 3055(w) (aromatic C═C-H), 2930, 2850 (w)(aliphatic C-H); 1645(s) (C═O, amide I); 1485, 1440(s) (aromatic C═C); 1400(m), 735, 695(s) (monosubstituted aromatic C-H); ^1H NMR: see Table 13; ^{13}C NMR: see Table 14. MS(+ES), *m/z* (RI%): 766(4)[M + $2Na^+$], 759(3)[M + K^+], 743(7)[M + Na^+], 721(4)[M + 1], 243(100)[Tr^+].

***N,N′*-[Dimethyl-(2,2′-dithiobisacetyl)]ethylenediamine (1)**

This synthesis was a modification of the method of Kamber (16). Resublimed I_2 (848 mg, 1.1 equiv., 3.30 mmol) was added to a solution of tritylthio ether **4** (1.16 mg, 3.00 mmol) in a degassed 2:1 v/v mixture (1.5 L) of acetonitrile and absolute EtOH under a N_2 atmosphere. The amber solution was further degassed for 30 min under aspirator vacuum (15 Torr; 1 Torr = 133.3 Pa), vented to dry N_2 gas, and allowed to stir at room temperature. After 12 h, the solution was concentrated to 20 mL, diluted with doubly distilled H_2O, decolorized with 1.0 N $Na_2S_2O_3$, and extracted with diethyl ether. A white solid was seen at the solvent interface. The organic phase was decanted and, after salting the aqueous layer, the precipitate was extracted into $CHCl_3$ and dried over $MgSO_4$ for 2 h. Filtration and rotary evaporation of the filtrate afforded an off-white, semi-solid (466 mg, 66%). The residue was suspended in isopropyl alcohol, chilled at −15°C, and filtered to separate most of the insoluble trityl carbinol. Recrystallization from peroxide-free THF gave opaque, non-geometric plates; mp 139.0–140.0°C; R_f 0.49 (10% MeOH in CH_2Cl_2); IR(KBr pellet): 2930, 2853 (m)(C-H); 1629 (s) (C═O, amide I); 1458 (m); 1396 (m); Raman: 645 (m)(CH_2-S), 510 (s)(S-S); ^1H NMR: see Table 1; ^{13}C NMR: see Table 2; MS(+NH_3 DCI), *m/z*(RI%): 252(100)[M + 18], 235(48)[M + 1], 205(10).

Acknowledgements

The authors gratefully acknowledge the financial support of the Natural Sciences and Engineering Research Council of Canada. We also thank Drs. A.D. Bain, D.W. Hughes, J.D. Laposa, L. Li, and M.J. McGlinchey for helpful discussions.

References

1. M.K. Dewanjee. Semin. Nucl. Med. **20**, 5, (1990).
2. D. Eshima, A.R. Fritzburg, and A. Taylor, Jr. Semin. Nucl. Med. **20**, 28 (1990).
3. H.F. Kung. Semin. Nucl. Med. **20**, 150 (1990).
4. W.C. Klingensmith III, A.R. Fritzburg, V.M. Spitzer, D.L. Johnson, C.C. Kuni, M.R. Williamson, G. Washer, and R. Weil. J. Nucl. Med. **25**, 42 (1984).
5. A.R. Fritzburg, P.G. Abrams, P.L. Beaumier, S. Kasina, A.C. Morgan, T.N. Reno, J.A. Sanderson, A. Srinivasan, D.S. Wilbur, and J.-L. Vanderheyden. Proc. Natl. Acad. Sci. U.S.A. **85**, 4025 (1988).
6. A. Capretta, R.B. Maharajh, and R.A. Bell. Carbohydr. Res. **267**, 49 (1995).
7. J.G. McAfee. *In* Radiopharmaceuticals. *Edited by* G. Subramanian, B.A. Rhodes, J.F. Cooper, and V.J. Sodd. The Society of Nuclear Medicine Inc., New York. 1975.
8. E. Livini, M.A. Davis, and V.D. Warner. J. Med. Chem. **22**, 580 (1979).
9. M.D. Loberg, E.H. Corder, A.T. Fields, and P.S. Callery. J. Nucl. Med. **20**, 1181 (1979).
10. B. Ivanov, W. Grzesik, and F.A. Robey. Bioconjugate Chem. **6**, 269 (1995).
11. T. W. Greene. Protecting groups in organic chemistry. J. Wiley, New York. 1981. p. 320.
12. D. Brenner, A. Davison, J. Lister-James, and A.G. Jones. Inorg. Chem. **23**, 3793 (1984).
13. S.Z. Lever, K.E. Baidoo, A.V. Kramer, and H.D. Burns. Tetrahedron Lett. **29**, 3219, 1988.
14. J. Xan, E.A. Wilson, L.D. Roberts, and N.H. Horton. J. Am. Chem. Soc. **63**, 1139 (1941).
15. R.H. Mach, H.F. Kung, P. Jungwiwattanaporn, and Y.-Z. Guo. Tetrahedron Lett. **30**, 4069 (1989).
16. B. Kamber. Helv. Chim. Acta, **54**, 417 (1971).
17. R.J. Abraham and P. Loftus. Proton and carbon-13 NMR spectroscopy — an integrated approach. Heyden, London. 1979. p. 169.

18. T.H. Siddhall and W.E. Stewart. J. Chem. Phys. **48**, 2928 (1968).
19. G. Claeson, G. Androes, and M. Calvin. J. Am. Chem. Soc. **83**, 9357 (1961).
20. C.H. Bushweller and M.H. Gianni. *In* The chemistry of ethers, crown ethers, hydroxyl groups and their sulphur analogues. Part 1. *Edited by* S. Patai. Interscience, Chichester. 1980. pp. 221–222.
21. M.B. Robin, F.A. Bovey, and H. Basch. *In* The chemistry of amides. *Edited by* S. Patai and J. Zabicky. Interscience, New York. 1970. p. 21.
22. F. Bohlmann and D. Schumann. Tetrahedron. Lett. **28**, 2435 (1965).
23. J. Dale and K. Titlestad. J. Chem. Soc. Chem. Commun. 656 (1969).
24. Z. Lidert. Tetrahedron, **27**, 967 (1981).
25. L.M. Jackman and S. Sternhell. Applications of nuclear magnetic resonance spectroscopy in organic chemistry. 2nd ed. Pergamon Press, Oxford. 1969. p. 91.
26. D. Neuhaus and M. Williamson. The nuclear Overhauser effect in structural and conformational analysis. VCH Publishers, New York. 1989. pp. 143–148.
27. S. Gronowitz and Z. Lidert. Chem. Scr. **16**, 97 (1980), and refs. therein.
28. W.E. Stewart and T.H. Siddall III. Chem. Rev. **70**, 517 (1970).
29. M. Frucht, A.H. Lewin, and F.A. Bovey. Tetrahedron Lett. **42**, 3707 (1970).
30. J.V. Hatton and R.E. Richards. Mol. Phys. **5**, 139 (1963). 31. L.A. LaPlanche and M.T. Rogers. J. Am. Chem. Soc. **85**, 3728 (1963).
32. L.L. Graham and M.R. Miller. Org. Magn. Reson. **4**, 327 (1972).
33. R.C Weast (*Editor*). CRC handbook of chemistry and physics. 68th ed. CRC Press, Boca Raton, Fla. 1987. p. D-188.
34. J.P. Idoux, J.M. Scandrett, and J.A. Sikorski. J. Am. Chem. Soc. **99**, 4577 (1977).
35. T.H. Siddall III, W.E. Stewart, and A.L. Marston. J. Phys. Chem. **72**, 2135 (1968).
36. M.A. Cremonini, L. Lunazzi, G. Placucci, R. Okazaki, and G. Yamamoto. J. Am. Chem. Soc. **112**, 2915 (1990).
37. J. Sandrström. Dynamic NMR spectroscopy. Academic Press, London. 1982. pp. 77, 86–91.
38. G. Claeson, G. Androes, and M. Calvin. J. Am. Chem Soc. **83**, 4357 (1961).
39. C.H. Bushweller, J. Golini, G. Rao, and J.W. O'Neil. J. Am. Chem. Soc. **92**, 3055 (1970).
40. A. Komornicki and J.W. McIver. J. Am. Chem. Soc. **95**, 4512 (1973).
41. O. Foss. *In* Organic sulfur compounds. Vol I. *Edited by* N. Kharash. Pergamon Press, New York. 1961. p. 77.
42. R. Rahman, S. Safe, and A. Taylor. Qt. Rev. **24**, 208 (1970).
43. A. Lidén, C. Roussel, T. Liljefors, M. Chanon, R.E. Metzger, and J. Sandström. J. Am. Chem. Soc. **98**, 2853 (1976).
44. M. Barfield, A.M. Dean, C.J. Fallick, R.J. Spear, S. Sternhell, and P.W. Westerman. J. Am. Chem. Soc. **97**, 1482 (1975).
45. V.G. Malkin, O.L. Malkina, L.A. Eriksson, and D.R. Salahub. *In* Theoretical and computational chemistry. Vol 2. *Edited by* J.M. Seminario and P. Politzer. Elsevier Science, B.V., New York. 1995. p. 273.
46. D.B. Chesnut. Annu. Rep. NMR. Spectrosc. **29**, 71 (1994); J. Gauss, M. Hofmann, and P.v.R. Schleyer. J. Am. Chem. Soc. **115**, 12385 (1993), and refs. therein.
47. R.F. Zürcher. *In* Progress in NMR spectroscopy. Vol II. *Edited by* J.W. Emsley, J. Feeney, and L.H. Sutcliffe. Pergamon Press, Oxford. 1967. p. 205.
48. H.M. McConnell. J. Chem. Phys. **27**, 226 (1957).
49. A.D. Buckingham. Can. J. Chem. **38**, 300 (1960).
50. N.J. Clayden and R.J.P. Williams. J. Magn. Reson. **49**, 383 (1982).
51. S. Winstein, P. Carter, F.A.L. Anet, and A.J.R. Bourn. J. Am. Chem. Soc. **87**, 5247 (1965).
52. S. Li and N.L. Allinger. Tetrahedron, **44**, 1339 (1988).
53. D.B. Chestnut and W.P. Johnson. J. Magn. Reson. **65**, 110 (1985).
54. B. Staskun. J. Org. Chem. **46**, 1643 (1981).
55. W.C. Still, M. Kahn, and A.J. Mitra. J. Org. Chem. **43**, 2923 (1978).
56. N. Walker and D. Stuart. Acta Crystallogr. Sect. A: Found. Crystallogr. **A39**, 158 (1983).
57. A.J.C. Wilson (*Editor*). International tables for cystallography. Vol. C. Kluwer Academic Publishers, Dordrecht. 1992. pp. 477–87.
58. SHELXTL PC. Version 4.1. Siemens Analytical X-Ray Instruments, Inc., Madison, Wis. May, 1990.
59. A. Bax. J. Magn. Reson. **53**, 517 (1983).
60. V. Rutar. J. Magn. Reson. **58**, 306 (1984).
61. J.A. Wilde and P.H. Bolton. J. Magn. Reson. **59**, 343 (1984).
62. C.A.G. Haasnoot, F.A.A.M. de Leeuw, and C. Altona. Tetrahedron, **36**, 2783 (1980).
63. M. Saunders, K.N. Houk, Y.-D. Wu, W.C. Still, M. Lipton, G. Chang, and W.C. Guida. J. Am. Chem. Soc. **112**, 1419 (1990).
64. PCMODEL user's guide. Version 4.0. Serena Software, Bloomington, Ind. p. 32.
65. M.J. Frisch, G.W. Trucks, H.B. Schlegel, P.M.W. Gill, B.G. Johnson, M.A. Robb, J.R. Cheeseman, T. Keith, G.A. Petersson, J.A. Montgomery, K. Raghavachari, M.A. Al-Laham, V.G. Zakrewski, J.V. Oortiz, J.B. Foresman, C.Y. Peng, P.Y. Ayala, W. Chen, M.W. Wong, J.L. Andres, E.S. Replogle, R. Gomperts, R.L. Martin, D.J. Fox, J.S. Binkley, D.J. Defrees, J. Baker, J.P. Stewart, M. Head-Gordon, C. Gonzalez, and J.A. Pople. Gaussian 94. Gaussian, Inc., Pittsburgh, Pa. 1994.
66. A.D. Becke. J. Chem. Phys. **98**, 5648 (1993).
67. P.J. Stevens, F.F. Devlin, C.F. Chabalowski, and M.J. Frisch. J. Phys. Chem. **98**, 11623 (1994).
68. K. Wolinski, J.F. Hilton, and P. Pulay. J. Am. Chem. Soc. **112**, 8251 (1990).